1 Remote Sensing: Basic Principles

> Electromagnetic radiation is just basically mysterious.
>
> B.K. Ridley, *Time, Space and Things*, 2nd edition. Cambridge University Press, Cambridge, 1984.

1.1 Introduction

The science of remote sensing consists of the analysis and interpretation of measurements of electromagnetic radiation (EMR) that is reflected from or emitted by a target and observed or recorded from a vantage point by an observer or instrument that is not in contact with the target. Earth observation by remote sensing (EO) is the interpretation and understanding of measurements made by airborne or satellite-borne instruments of EMR that is reflected from or emitted by objects on the Earth's land, ocean or ice surfaces or within the atmosphere, together with the establishment of relationships between these measurements and the nature and distribution of phenomena on the Earth's surface or within the atmosphere. Figure 1.1 shows in schematic form the various methods of computer processing (blue boxes) that generate products (green boxes) from remotely-sensed data. This book deals with the methods of computer processing of remotely sensed data (the green and blue boxes) as well as providing an introduction to environmental geographical information systems (E-GISs) (Chapter 10) which make use of remotely-sensed products.

Remotely-sensed images are often used as image maps or backcloths for the display of spatial data in an E-GIS. Methods of improving the appearance of an image (termed *enhancement* procedures) are dealt with in Chapters 4, 5 and 7. Chapter 8 is an introduction to *pattern recognition* techniques that produce labelled images in which each type of land use, for example is represented by a numeric code (for example 1 = broadleaved forest, 2 = water, and so on.). These labelled images can provide free-standing information or can be combined with other spatial data within an E-GIS. Properties of earth surface materials, such as soil moisture content, sea surface temperature (SST) or biomass can be related to remotely sensed measurements using statistical methods. For instance, a sample of measurements of soil moisture content can be collected close to the time of satellite overpass and the corresponding ground reflectance or ground temperature that are recorded by the satellite's instruments can be related via regression analysis to the ground measurements. This sample relationship can then be applied to the entire area of interest. These bio-geophysical variables are used in environmental modelling, often within an E-GIS. Elevation models are another form of remotely-sensed spatial information that is used in E-GIS. Digital elevation models can be derived from optical imagery using two sensors, for example one pointing down and one pointing obliquely backwards (this is the case with the ASTER sensor, discussed in Chapter 2). Another way of producing elevation models is by the use of synthetic aperture radar (SAR) interferometry, which is discussed in Chapter 9. The increasing cooperation between remote sensing specialists and E-GIS users means that more products are available to E-GIS users and the more spatial information is combined with remotely sensed data to produce improved results. This is an example of synergy (literally, working together).

A fundamental principle underlying the use of remotely sensed data is that different objects on the Earth's surface and in the atmosphere reflect, absorb, transmit or emit electromagnetic energy (EME) in different proportions across the range of wavelengths known as the electromagnetic spectrum, and that such differences allow these objects to be identified uniquely. Sensors mounted on aircraft or satellite platforms record the magnitude of the energy flux reflected from or emitted by objects on the Earth's surface. These measurements are made at a large number of points distributed either along a one-dimensional profile on the ground below the platform or over a two-dimensional area below or to one side of the ground track of the platform. Figure 1.2a shows an image being collected by a nadir-looking sensor.

Data in the form of one-dimensional profiles are not considered in this book, which is concerned with

Computer Processing of Remotely-Sensed Images: An Introduction, Fourth Edition Paul M. Mather and Magaly Koch

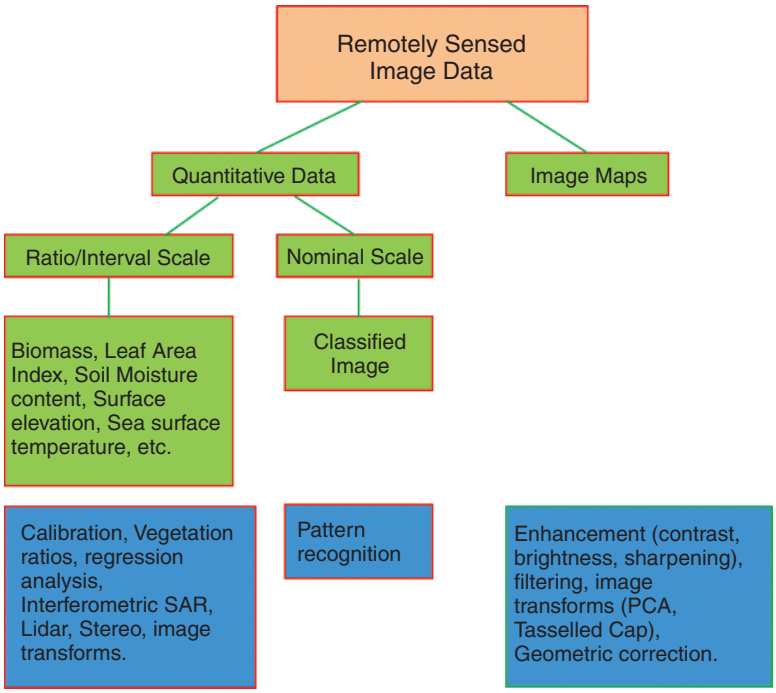

Figure 1.1 *Uses of remotely-sensed data. The green boxes show the products derived from remotely-sensed data, such as image maps and classified images. The blue boxes show the computer processing techniques that are used to derive these products. Image maps are frequently used as backdrops in a GIS, whereas the process of pattern recognition produces labelled (nominal scale) images showing the distribution of individual Earth surface cover types. Quantitative measures such as vegetation indices are derived from calibrated data, and are often linked via regression analysis to Earth surface properties such as sea-surface temperature or soil moisture content. The computer processing techniques to extract and analyse remotely-sensed data are presented in the remainder of this book.*

the processing of two-dimensional (spatial) data collected by imaging sensors. Imaging sensors are either nadir – (vertical) or side-looking. In the former case, the ground area to either side of the point immediately below the satellite or aircraft platform is imaged, while in the latter case an area of the Earth's surface lying to one side or other of the satellite or aircraft track is imaged. The most familiar kinds of images, such as those collected by the nadir-looking thematic mapper (TM) and enhanced thematic mapper plus (ETM+) instruments carried by US Landsat satellites numbered 5 and 7 (6 never reached orbit), and by the HRV instrument (which can be side-looking or nadir-pointing) on board the French/Belgian/Swedish SPOT satellites, are scanned line by line (from side to side) as the platform moves forwards along its track. This forward (or along track) motion of the satellite or aircraft is used to build up an image of the Earth's surface by the collection of successive scan lines (Figure 1.2a).

Two kinds of scanners are used to collect the EMR that is reflected or emitted by the ground surface along each scan line. Electromechanical scanners have a small number of detectors, and they use a mirror that moves back and forth to collect electromagnetic energy across the width of the scan line (AB in Figure 1.2a). The electromagnetic energy reflected by or emitted from the portion of the Earth's surface that is viewed at a given instant in time is directed by the mirror onto these detectors (Figure 1.2b). The second type of scanner, the push-broom scanner, uses an array of solid-state charge-coupled devices (CCDs), each one of which 'sees' a single point on the scan line (Figure 1.2c). Thus, at any given moment, each detector in the CCD array is observing a small area of the Earth's surface along the scan line. This ground area is called a pixel. A remotely-sensed image is made up of a rectangular matrix of measurements of the flux or flow of EMR emanating from individual pixels, so that each pixel value represents the magnitude of upwelling EMR for a small ground area (though it will be seen later that there is 'interference' from neighbouring pixels). This upwelling radiation contains information about (i) the nature of the Earth-surface material present in the pixel area, (ii) the topographic position of the pixel area (i.e. whether it is horizontal, on a sunlit slope or on a shaded slope) and (iii) the state of the atmosphere through which the EMR has to pass. This account of image acquisition is a very simplified one, and more detail is provided in Chapter 2. The nature of Earth-surface

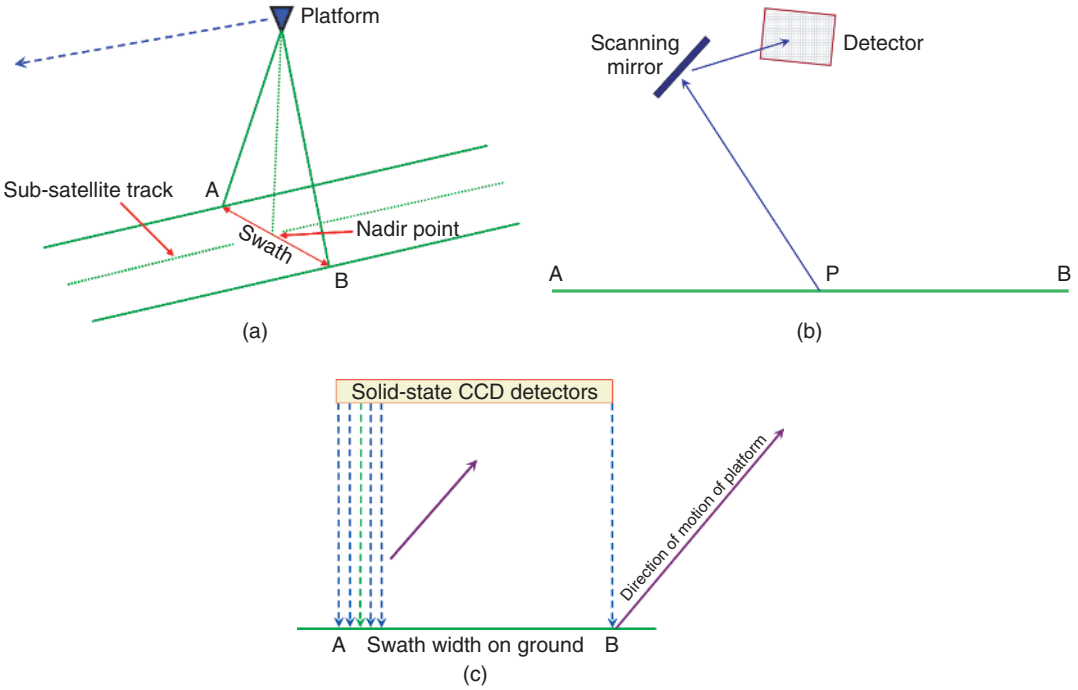

Figure 1.2 *(a) A sensor carried onboard a platform, such as an Earth-orbiting satellite, builds up an image of the Earth's surface by taking repeated measurements across the swath AB. As the satellite moves forward, so successive lines of data are collected and a two-dimensional image is generated. The distance AB is the swath width. The point immediately below the platform is the nadir point, and the imaginary line traced on the Earth's surface by the nadir point is the subsatellite track. (b) Upwelling energy from point P is deflected by a scanning mirror onto the detector. The mirror scans across a swath between points A and B on the Earth's surface. (c) An array of solid state (CCD) detectors images the swath AB. The image is built up by the forward movement of the platform.*

materials and their interaction with EMR is covered in Section 1.3. Topographic and atmospheric interactions are described in Sections 4.7 and 4.4, respectively.

The magnitude of the radiance reflected or emitted by the small ground area represented by a pixel is a physical measurement that is converted to a number, usually an integer (a whole number) lying within a specified range, such as 0–255 (8 bits) or 0–65 535 (16 bits). Remotely-sensed images thus consist of rectangular arrays of numbers, and because they are numerical in nature so computers are used to display, enhance and manipulate them. The main part of this book deals with techniques used in these types of processing. Spatial patterns evident in remotely-sensed images can be interpreted in terms of geographical variations in the nature of the material forming the surface of the Earth. These Earth surface materials may be vegetation, exposed soil and rock or water surfaces. Notice that the characteristics of these materials are not detected directly by remote sensing. Their nature is inferred from the properties of the EMR that is reflected, scattered or emitted by these materials and recorded by the sensor. Another characteristic of digital image data is that they can be calibrated in order to provide estimates of physical measurements of properties of the target such as radiance, reflection or albedo. These values are used, for example in models of climate or crop growth. Examples of the uses of remotely-sensed image data in Earth science and environmental management can be found in Calder (1991). Kaufman *et al.* (1998) demonstrate the wide variety of applications of remote sensing data collected by the instruments on the American Terra satellite. A number of web sites provide access to image libraries. Perhaps the most accessible of these is NASA's Earth Observatory. The Internet contains an ever-changing but large number of Earth-observation images that can be best discovered by using a search engine. Many national space agencies maintain good web sites, for example NASA (USA), CNES (France) and DLR (Germany).

Aerial photography is a familiar form of EO by remote sensing. Past generations of air photographs differ from digital images in that they are analogue in nature. Analogue means: using some alternative physical representation to display some property of interest. For example, a photographic film represents a range of light levels in terms of the differential response of silver halide particles in the film emulsion. Analogue images cannot be processed by computer unless they are converted to digital form, using a scanning device. Computer scanners

operate much in the same way as those carried by satellites in that they view a small area of the photograph, record the proportion of incident light that is reflected back by that small area and convert that proportion to a number, usually in the range 0 (no reflection, or black) to 255 (100% reflection, or white). The numbers between 0 and 255 represent increasingly lighter shades of grey.

Nowadays, analogue cameras are rarely used and digital cameras are most often chosen for use in aerial photography. Images acquired by such cameras are similar in nature to those produced by the pushbroom type of sensor mentioned above. Instead of a film, a digital camera has a two-dimensional array of charge-coupled devices (CCD) (rather than a one-dimensional CCD array, as used by the SPOT satellite's HRV instrument, mentioned above). The amount of light from the scene that impinges on an individual CCD is recorded as a number in the range 0 (no light) to 255 (detector saturated). A value of 255 is typically used as the upper bound of the range but a different value may be selected depending on the camera characeteristics. A two-dimensional set of CCD measurements produces a greyscale image. Three sets of CCDs are used to produce a colour image, just as three layers of film emulsion are used to generate an analogue colour photograph. The three sets of CCDs measure the amounts of red, green and blue light that reach the camera. Nowadays, digital imagery is relatively easily available from digital cameras, from scanned analogue photographs, as well as from sensors carried by aircraft, including unmanned drones (see Zhou *et al*., 2009) and satellites.

The nature and properties of EMR are considered in Section 1.2, and are those which concern its interaction with the atmosphere, through which the EMR passes on its route from the Sun (or from another source such as a microwave radar) to the Earth's surface and back to the sensor mounted onboard an aircraft or satellite. Interactions between EMR and Earth surface materials are summarized in Section 1.3. It is by studying these interactions that the nature and properties of the material forming the Earth's surface are inferred.

The topics covered in this book are dealt with to a greater or lesser extent in a number of textbooks, research monographs and review articles. A good library will provide paper or electronic access to a selection of recent texts that include: Adams and Gillespie (2006), Campbell (2006), Chuvieco (2008), Drury (2004), Elachi and van Zyl (2006), Gao (2009), Gonzales and Woods (2007), Jensen (1996), Landgrebe (2003), Liang (2004), Liang *et al*. (2008), Lillesand, Kiefer and Chipman (2008), Milman (1999), Olsen (2007), Rees (2001), Richards and Jia (2006), Schowengerdt (2006), Smith (2001), Warner, Nellis and Foody (2009) and Weng and Quattrochi (2007). Sanchez and Canton (1998) discuss both remote sensing and space telescope images, while Rees (2001) covers basic principles in a very understandable way. Trauth *et al*. (2007) contains MATLAB code and explanation of some of the topics mentioned in this book, including image processing, DEM manipulation and geostatistics. Some of the material listed above is not written specifically for a remote sensing audience, but nevertheless, contain useful and often additional reading for those readers wishing to follow up a particular topic for a thesis or dissertation. The above list of books and articles may seem to be lengthy, but some readers may prefer to avoid an overtly mathematical approach and thus select one source rather than another.

1.2 Electromagnetic Radiation and Its Properties

1.2.1 Terminology

The terminology used in remote sensing is sometimes understood only imprecisely, and is therefore occasionally used loosely. A brief guide is therefore given in this section. It is neither complete nor comprehensive, and is meant only to introduce some basic ideas. The subject is dealt with more thoroughly by Bird (1991a, b), Chapman (1995), Hecht (2001), Kirkland (2007), Martonchik, Bruegge and Strahler (2000), Nicodemus *et al*. (1977), Rees (2001), Schaepman-Strub *et al*. (2006), Slater (1980), Smith (2001) and the references listed at the end of the preceding section.

EMR transmits energy. As the name implies, EMR has two components. One is the electric field and the other is the magnetic field. These two fields are mutually perpendicular, and are also perpendicular to the direction of travel (Figure 1.3). There is no 'right way up' – EMR can be transmitted with a horizontal electric field and a vertical magnetic field, or vice versa. The disposition of the two fields is described by the polarization state of the EMR, which can be either horizontal or vertical. Polarization state is used in microwave remote sensing (Section 2.4).

Energy is the capacity to do work. It is expressed in joules (J), a unit that is named after James Prescott Joule, an English brewer whose hobby was physics. *Radiant energy* is the energy associated with EMR. The rate of transfer of energy from one place to another (for example from the Sun to the Earth) is termed the *flux* of energy, the word *flux* being derived from the Latin word meaning 'flow'. It is measured in watts (W), after James Watt (1736–1819), the Scottish inventor who was instrumental in designing an efficient steam engine while he was working as a technician at Glasgow University (he is also credited with developing the first rev counter). The interaction between EMR and surfaces such as that of the Earth can be understood more clearly if the concept of

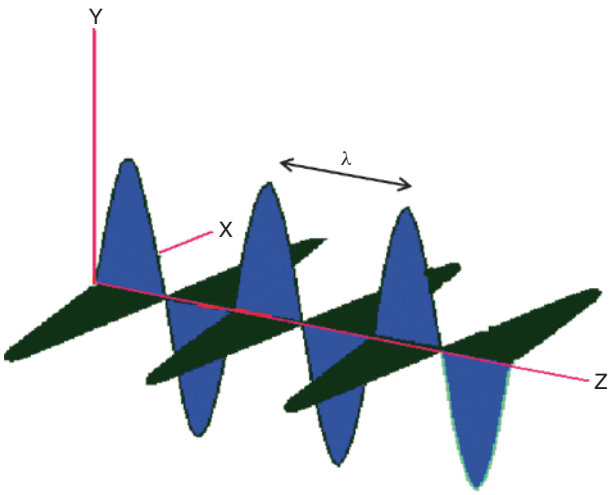

Figure 1.3 *Electromagnetic wave. The wavelength of the electromagnetic energy is represented by the Greek letter lambda (λ). Adapted from a figure by Nick Strobel, from http://www.astronomynotes.com/light/s2.htm. Accessed 24 May 2010.*

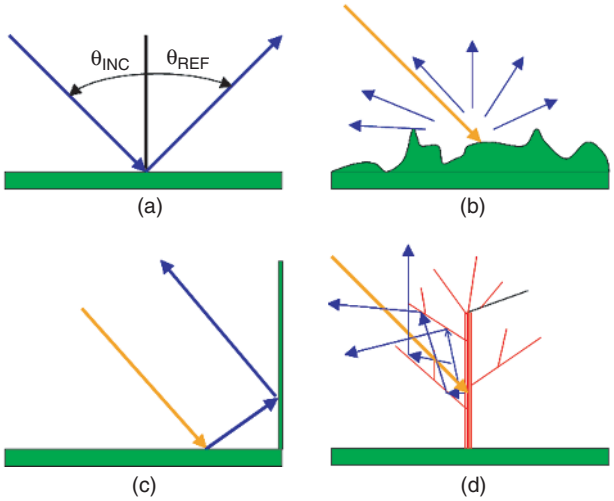

Figure 1.4 *Types of scattering of electromagnetic radiation. (a) Specular, in which incident radiation is reflected in the forward direction, (b) Lambertian, in which incident radiation is equally scattered in all upward directions, (c) corner reflector, which acts like a vertical mirror, especially at microwave wavelengths and (d) volume scattering, in which (in this example) branches and leaves produce single-bounce (primary) and multiple-bounce (secondary) scattering.*

radiant flux density is introduced. Radiant flux is the rate of transfer of radiant (electromagnetic) energy. Density implies variability over the two-dimensional surface on which the radiant energy falls, hence radiant flux density is the magnitude of the radiant flux that is incident upon or, conversely, is emitted by a surface of unit area (measured in watts per square metre or $W\,m^{-2}$). The topic of emission of EMR by the Earth's surface in the form of heat is considered at a later stage. If radiant energy falls (i.e. is incident) upon a surface then the term *irradiance* is used in place of radiant flux density. If the energy flow is away from the surface, as in the case of thermal energy emitted by the Earth or solar energy that is reflected by the Earth, then the term *radiant exitance* or *radiant emittance* (measured in units of $W\,m^{-2}$) is appropriate.

The term *radiance* is used to mean the radiant flux density transmitted from a unit area on the Earth's surface as viewed through a unit solid (three-dimensional) angle (just as if you were looking through a hole at the narrow end of an ice-cream cone). This solid angle is measured in *steradians*, the three-dimensional equivalent of the familiar radian (defined as the angle subtended at the centre of a circle by a sector which cuts out a section of the circumference that is equal in length to the radius of the circle). If, for the moment, we consider that the irradiance reaching the surface is back-scattered in all upward directions (Figure 1.4), then a proportion of the radiant flux would be measured per unit solid viewing angle. This proportion is the radiance (Figure 1.5). It is measured in watts per square metre per steradian ($W\,m^{-2}\,sr^{-1}$). The concepts of the radian and steradian are illustrated in Figure 1.6.

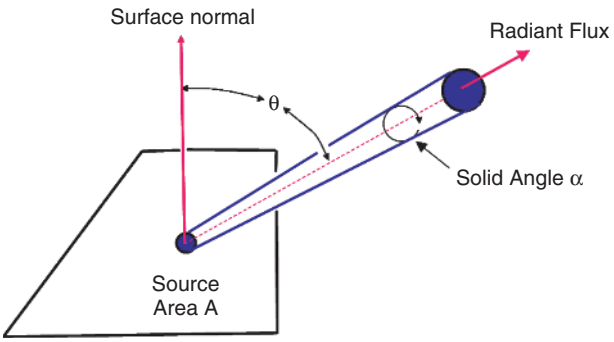

Figure 1.5 *Radiance is the flux of electromagnetic energy leaving a source area A in direction θ per solid angle α. It is measured in watts per square metre per steradian ($W\,m^{-2}\,sr^{-1}$).*

Reflectance, ρ, is the dimensionless ratio of the radiant emittance of an object and the irradiance. The reflectance of a given object is independent of irradiance, as it is a ratio. When remotely-sensed images collected over a time period are to be compared it is common practice to convert the radiance values recorded by the sensor into reflectance factors in order to eliminate the effects of variable irradiance over the seasons of the year. This topic is considered further in Section 4.6.

The quantities described above can be used to refer to particular wavebands rather than to the whole electromagnetic spectrum (Section 1.2.3). The terms are then preceded by the adjective *spectral;* for example the spectral

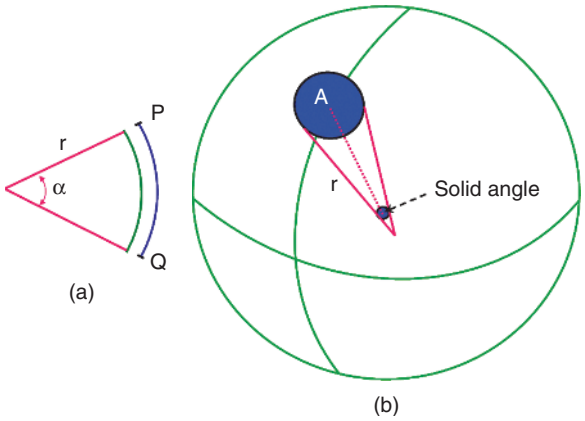

Figure 1.6 *(a) The angle α formed when the length of the arc PQ is equal to the radius of the circle r is equal to 1 radian or approximately 57°. Thus, angle α = PQ/r radians. There are 2π radians in a circle (360°). (b) A steradian is a solid three-dimensional angle formed when the area A delimited on the surface of a sphere is equal to the square of the radius r of the sphere. A need not refer to a uniform shape. The solid angle shown is equal to A/r² steradians (sr). There are 4π steradians in a sphere.*

radiance for a given waveband is the radiant flux density in that waveband (i.e. spectral radiant flux density) per unit solid angle. Terms such as *spectral irradiance*, *spectral reflectance* and *spectral exitance* are defined in a similar fashion.

1.2.2 Nature of Electromagnetic Radiation

An important point of controversy in physics over the last 300 years has concerned the nature of EMR. Newton, while not explicitly rejecting the idea that light is a wave-like form of energy (the wave theory) inclined to the view that it is formed of a stream of particles (the corpuscular theory). The wave–corpuscle dichotomy was not to be resolved until the early years of the twentieth century with the work of Planck, Einstein and others. The importance to remote sensing of the nature of EMR is fundamental, for we need to consider radiation both as a waveform and as a stream of particles. The wave-like characteristics of EMR allow the distinction to be made between different manifestations of such radiation (for example microwave and infrared (IR) radiation) while, in order to understand the interactions between EMR and the Earth's atmosphere and surface, the idea that EMR consists of a stream of particles is most easily used. Building on the work of Planck, Einstein proposed in 1905 that light consists of particles called *photons*, which, in most respects, were similar to other sub-atomic particles such as protons and neutrons. It was found that, at the subatomic level, both wave-like and particle-like properties were exhibited, and that phenomena at this level appear to be both waves and particles. Erwin Schrödinger (1867–1961) wrote as follows in *Science, Theory and Man* (New York, Dover, 1957):

> In the new setting of ideas, the distinction [between particles and waves] has vanished, because it was discovered that all particles have also wave properties, and vice-versa. Neither of the concepts must be discarded, they must be amalgamated. Which aspect obtrudes itself depends not on the physical object but on the experimental device set up to examine it.

Thus, from the point of view of quantum mechanics, EMR is both a wave and a stream of particles. Whichever view is taken will depend on the requirements of the particular situation. In Section 1.2.5, the particle theory is best suited to explain the manner in which incident EMR interacts with the atoms, molecules and other particles which form the Earth's atmosphere. Readers who, like myself, were resistant in their formative years to any kind of formal training in basic physics will find Gribben (1984) to be readable as well as instructive, while Feynman (1985) is a clear and well-illustrated account of the surprising ways that light can behave.

1.2.3 The Electromagnetic Spectrum

The Sun's light is the form of EMR that is most familiar to human beings. Sunlight that is reflected by physical objects travels in most situations in a straight line to the observer's eye. On reaching the retina, it generates electrical signals that are transmitted to the brain by the optic nerve. The brain uses these signals to construct an image of the viewer's surroundings. This is the process of vision, which is closely analogous to the process of remote sensing; indeed, vision is a form – perhaps the basic form – of remote sensing (Greenfield, 1997). A discussion of the human visual process can be found in Section 5.2. Note that the process of human vision involves image acquisition (essentially a physiological process) and image understanding (a psychological process), just as EO by remote sensing does. Image interpretation and understanding in remote sensing might therefore be considered to be an attempt to simulate or emulate the brain's image understanding functions.

Visible light is so called because the eye detects it, whereas other forms of EMR are invisible to the unaided eye. Sir Isaac Newton (1643–1727) investigated the nature of white light, and in 1664 concluded that it is made up of differently coloured components, which he saw by passing white light through a prism to form a rainbow-like spectrum. Newton saw the *visible spectrum*, which ranges from red through orange, yellow and green to blue, indigo and violet. Later, the astronomer Friedrich Wilhelm (Sir William) Herschel (1728–1822)

demonstrated the existence of EMR with wavelengths beyond those of the visible spectrum; these he called *infrared*, meaning *beyond the red*. It was subsequently found that EMR also exists beyond the violet end of the visible spectrum, and this form of radiation was given the name *ultraviolet*. (Herschel, incidentally, started his career as a band-boy with the Hanoverian Guards and later came to live in England.)

Other forms of EMR, such as X-rays and radio waves, were discovered later, and it was eventually realized that all were manifestations of the same kind of radiation which travels at the speed of light in a wave-like form, and which can propagate through empty space. The speed of light (c_0) is 299 792 458 m s^{-1} (approximately 3×10^8 m s^{-1}) in a vacuum, but is reduced by a factor called the index of refraction if the light travels through media such as the atmosphere or water. EMR reaching the Earth comes mainly from the Sun and is produced by thermonuclear reactions in the Sun's core. The set of all electromagnetic waves is called the *electromagnetic spectrum*, which includes the range from the long radio waves, through the microwave and IR wavelengths to visible light waves and beyond to the ultraviolet and to the short-wave X and γ rays (Figure 1.7).

Symmetric waves can be described in terms of their *frequency* (f), which is the number of waveforms passing a fixed point in unit time. This quantity used to be known as *cycles per second* (cps) but nowadays the preferred term is Hz (Hertz, after Heinrich Hertz (1857–1894), who, between 1885 and 1889 became the first person to broadcast and receive radio waves). Alternatively, the concept of *wavelength* can be used (Figure 1.8). The wavelength is the distance between successive peaks (or successive troughs) of a waveform, and is normally measured in metres or fractions of a metre (Table 1.1). Both frequency and wavelength convey the same information and are often used interchangeably. Another measure of the nature of a waveform is its period (T). This is the time, in seconds, needed for one full wave to pass a fixed point. The relationships between wavelength, frequency and period are given by:

$$f = c/\lambda$$

$$\lambda = c/f$$

$$T = 1/f = \lambda/c$$

In these expressions, c is the speed of light. The velocity of propagation (v) is the product of wave frequency and wavelength, that is

$$v = \lambda f$$

The *amplitude* (A) of a wave is the maximum distance attained by the wave from its mean position (Figure 1.8). The amount of energy, or intensity, of the waveform

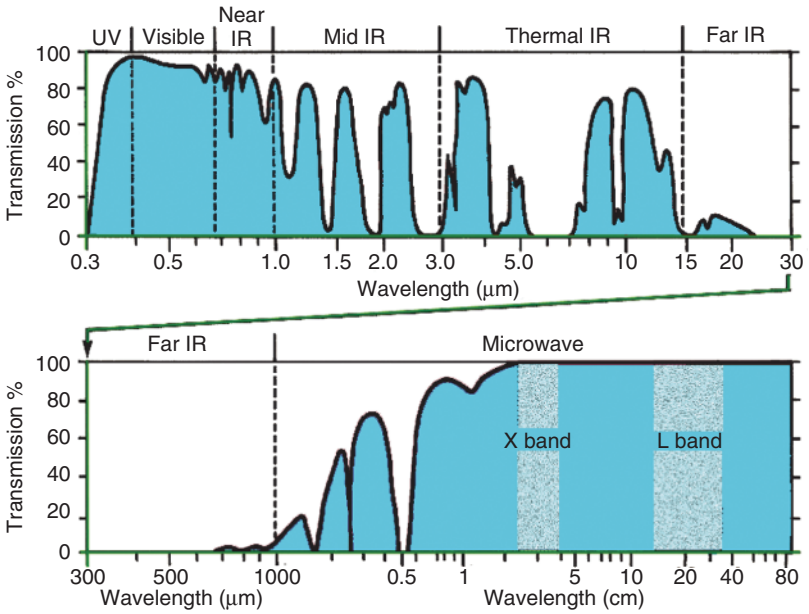

Figure 1.7 *The electromagnetic spectrum showing the range of wavelengths between 0.3 μm and 80 cm. The vertical dashed lines show the boundaries of wavebands such as ultraviolet (UV) and near-infrared (near IR). The shaded areas between 2 and 35 cm wavelength indicate two microwave wavebands (X band and L band) that are used by imaging radars. The curve shows atmospheric transmission. Areas of the electromagnetic spectrum with a high transmittance are known as atmospheric windows. Areas of low transmittance are opaque and cannot be used to remotely sense the Earth's surface. Reprinted from AFH Goetz and LC Rowanm 1981, Geologic Remote Sensing, Science,* ***221****, 781–791, Figure 1.*

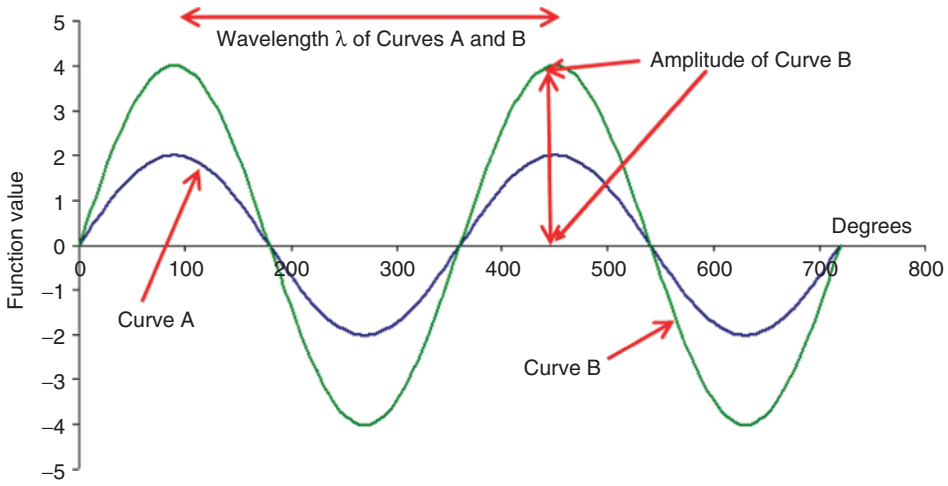

Figure 1.8 *Two curves (waveforms) A and B have the same wavelength (360° or 2π radians, x-axis). However, curve A has an amplitude of two units (y-axis) while curve B has an amplitude of four units. If we imagine that the two curves repeat to infinity and are moving to the right, like traces on an oscilloscope, then the frequency is the number of waveforms (0–2π) that pass a fixed point in unit time (usually measured in cycles per second or Hertz, Hz). The period of the waveform is the time taken for one full waveform to pass a fixed point. These two waveforms have the same wavelength, frequency and period and differ only in terms of their amplitude.*

Table 1.1 *Terms and symbols used in measurement.*

Factor	Prefix	Symbol	Factor	Prefix	Symbol
10^{-18}	atto	a	–	–	–
10^{-15}	femto	f	10^{15}	peta	P
10^{-12}	pico	p	10^{12}	tera	T
10^{-9}	nano	n	10^{9}	giga	G
10^{-6}	micro	μ	10^{6}	mega	M
10^{-3}	milli	m	10^{3}	kilo	k

is proportional to the square of the amplitude. Using the relationships specified earlier we can compute the frequency given the wavelength, and vice versa. If, for example wavelength λ is 0.6 μm or 6×10^{-7} m, then, since velocity v equals the product of wavelength and frequency f, it follows that:

$$v = 6 \times 10^{-7} f$$

so that:

$$f = \frac{c_0}{v} = \frac{3 \times 10^8}{6 \times 10^{-7}} \text{ Hz}$$

that is

$$f = 0.5 \times 10^{15} \text{Hz} = 0.5 \text{ PHz}$$

1 PHz (petahertz) equals 10^{15} Hz (Table 1.1). Thus, EMR with a wavelength of 0.6 μm has a frequency of 0.5×10^{15} Hz. The *period* is the reciprocal of the frequency, so one wave of this frequency will pass a fixed point in 2×10^{-15} s. The amount of energy carried by the waveform, or the squared amplitude of the wave, is defined for a single photon by the relationship

$$E = hf$$

where E is energy, h is a constant known as Planck's constant (6.625×10^{-34} J s) and f is frequency. Energy thus increases with frequency, so that high frequency, short-wavelength EMR such as X-rays carries more energy than does longer-wavelength radiation in the form of visible light or radio waves.

While EMR with particular temporal and spatial properties is used in remote sensing to convey information about a target, it is interesting to note that both time and space are defined in terms of specific characteristics of EMR. A second is the duration of 9 192 631 770 oscillations of the caesium radiation (in other words, that number of wavelengths or cycles are emitted by caesium radiation in 1 s; its frequency is approximately 9 GHz or a wavelength of around 0.03 m). A metre is defined as 1 650 764.73 vacuum wavelengths of the orange–red light emitted by krypton-86.

Visible light is defined as electromagnetic radiation with wavelengths between (approximately) 0.4 and 0.7 μm. We call the shorter wavelength end (0.4 μm) of the visible spectrum 'blue' and the longer wavelength end (0.7 μm) 'red' (Table 1.2). The eye is not uniformly sensitive to light within this range, and has its peak sensitivity at around 0.55 μm, which lies in the green part of the visible spectrum (Figure 1.7 and Figure 1.9). This peak in the response function of the human eye

Table 1.2 *Wavebands corresponding to perceived colours of visible light.*

Colour	Waveband (μm)	Colour	Waveband (μm)
Red	0.780 to 0.622	Green	0.577 to 0.492
Orange	0.622 to 0.597	Blue	0.492 to 0.455
Yellow	0.597 to 0.577	Violet	0.455 to 0.390

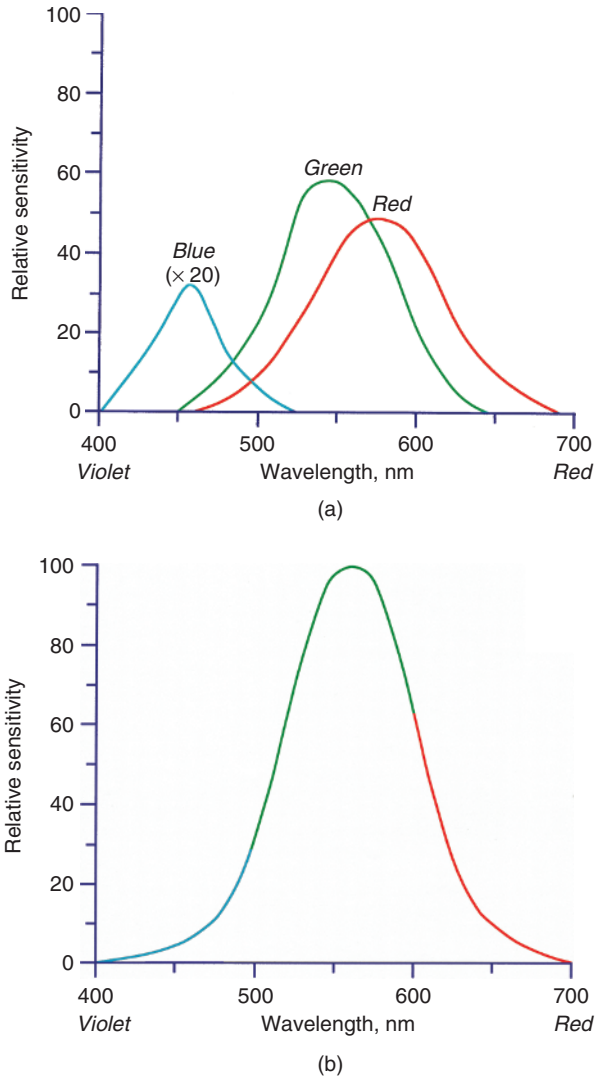

Figure 1.9 *(a) Response function of the red-, green- and blue-sensitive cones on the retina of the human eye. (b) Overall response function of the human eye. Peak sensitivity occurs near 550 nm (0.55 μm).*

corresponds closely to the peak in the Sun's radiation emittance distribution (Section 1.2.4).

The process of atmospheric scattering, discussed in Section 1.2.5 below, deflects light rays from a straight path and thus causes blurring or haziness. It affects the blue end of the visible spectrum more than the red end, and consequently the blue wave and is not used in many remote-sensing systems.

Figure 1.10a–c shows three greyscale images collected in the blue/green, green and red wavebands respectively by a sensor called the Thematic Mapper that is carried by the American Landsat-5 and Landsat-7 satellites (Chapter 2). The different land cover types reflect energy in the visible spectrum in a differential manner, although the clouds and cloud shadows in the upper centre of the image are clearly visible in all three images. Various crops in the fields round the village of Littleport (north of Cambridge in eastern England) can be discriminated, and the River Ouse can also be seen as it flows northwards in the right hand side of the image area. It is dangerous to rely solely on visual interpretation of images such as these. This book is about the processing and manipulation of images, and we will see that it is possible to change the colour balance, brightness and contrast of images to emphasize (or de-emphasize) particular targets. Digital image processing should be an aid to interpretation, but the user should always be aware of enhancements that have been carried out.

EMR with wavelengths shorter than those of visible light (less than 0.4 μm) is divided into three spectral regions, called γ rays, X-rays and ultraviolet radiation. Because of the effects of atmospheric scattering and absorption (Section 4.4; Figure 4.11), none of these wavebands is used in satellite remote sensing, though low-flying aircraft can detect γ-ray emissions from radioactive materials in the Earth's crust. Radiation in these wavebands is dangerous to life, so the fact that it is mostly absorbed or scattered by the atmosphere allows life to exist on Earth. In terms of the discussion of the wave–particle duality in Section 1.2.2, it should be noted that γ radiation has the highest energy levels and is the most 'particle-like' of all EMR, whereas radio frequency radiation is most 'wave-like' and has the lowest energy levels.

Wavelengths that are longer than the visible red are subdivided into the IR, microwave and radio frequency wavebands. The IR waveband, extending from 0.7 μm to 1 mm, is not a uniform region. Short-wavelength infrared (SWIR) or near-infrared (NIR) energy, with wavelengths between 0.7 and 0.9 μm, behaves like visible light and can be detected by special photographic film. IR radiation with a wavelength of up to 3.0 μm is primarily of solar origin and, like visible light, is reflected by the surface of the Earth. Hence, these wavebands are often known as the *optical* bands. Figure 1.11a shows an image of the area shown in Figure 1.10 collected by the Landsat TM sensor in the NIR region of the spectrum (0.75 – 0.90 μm). This image is considerably clearer than the visible spectrum images shown in Figure 1.10. We will see in Section 1.3.2 that the differences in reflection

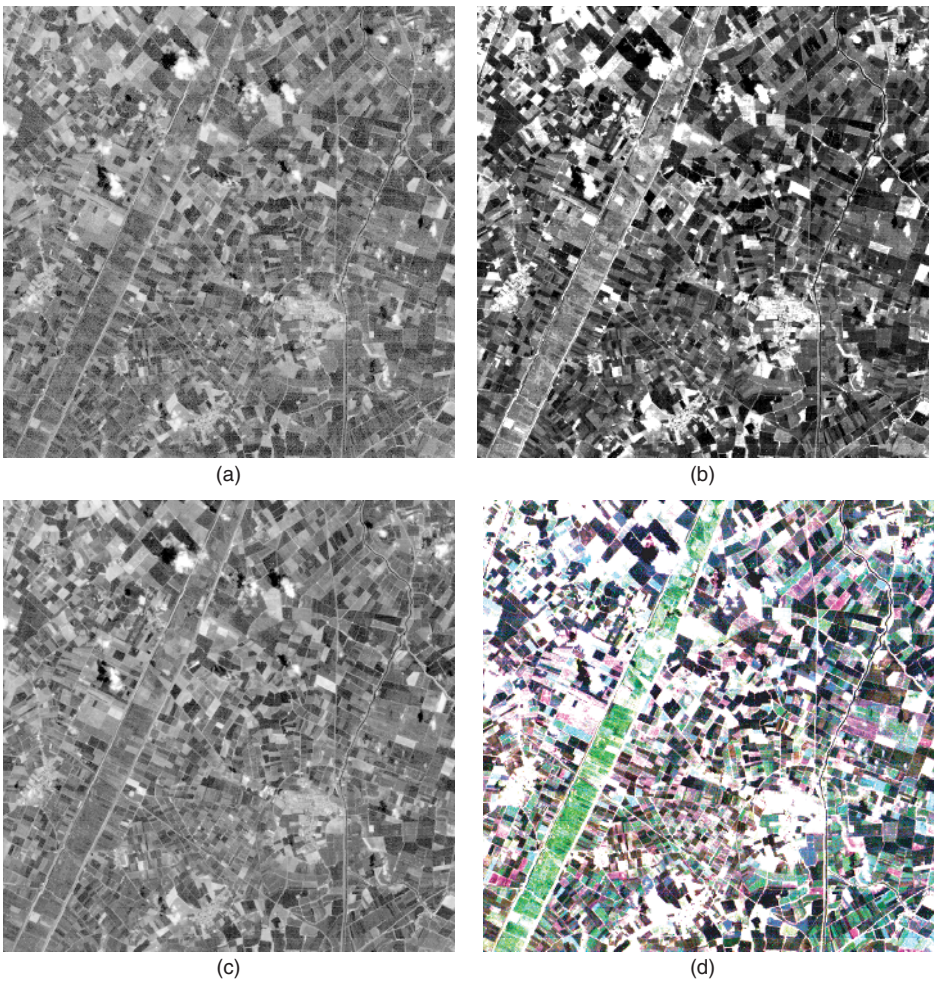

Figure 1.10 *Images collected in (a) band 1 (blue–green), (b) band 2 (green) and (c) band 3 (red) wavebands of the optical spectrum by the Thematic Mapper sensor carried by the Landsat-5 satellite. Image (d) shows the three images (a–c) superimposed with band 1 shown in blue, band 2 in green and band 3 in red. This is called a natural colour composite image. The area shown is near the town of Littleport in Cambridgeshire, eastern England. The diagonal green strip is an area of fertile land close to a river. Original data © ESA 1994; Distributed by Eurimage.*

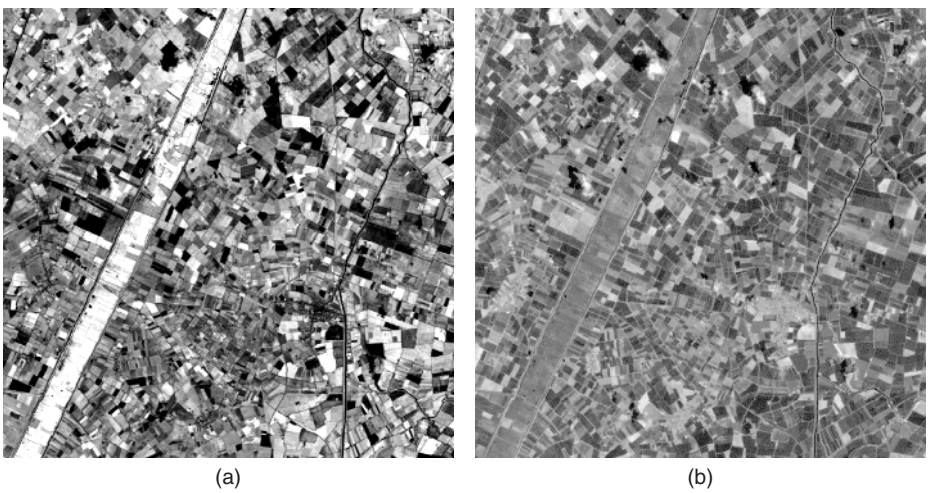

Figure 1.11 *Image of ground reflectance in (a) the 0.75–0.90 μm band (near infrared) and (b) the middle infrared (2.08–2.35 μm) image of the same area as that shown in Figure 1.10. These images were collected by the Landsat-5 Thematic Mapper (bands 4 and 7). Original data © ESA 1994; Distributed by Eurimage.*

between vegetation, water and soil are probably greatest in this NIR band. An image of surface reflection in the Landsat TM mid-IR waveband (2.08 – 2.35 µm) of the same area is shown in Figure 1.11b.

In wavelengths longer than around 3 µm, IR radiation emitted by the Earth's surface can be sensed in the form of heat. The amount and wavelength of this radiation depends on the temperature of the source (Section 1.2.4). Because these longer IR wavebands are sensed as heat, they are called the *thermal infrared* (TIR) wavebands. Much of the TIR radiation emitted by the Earth is absorbed by, and consequently heats, the atmosphere thus making life possible on the Earth (Figure 1.7). There is, however, a 'window' between 8 and 14 µm which allows a satellite sensor above the atmosphere to detect thermal radiation emitted by the Earth, which has its peak wavelength at 9.7 µm. Note, though, that the presence of ozone in the atmosphere creates a narrow absorption band within this window, centred at 9.5 µm. Boyd and Petitcolin (2004) consider remote sensing in the region 3.0 – 5.0 µm. There are a number of regions of high transmittance in this middle IR band, which is really a transition between reflected visible and NIR radiation and emitted TIR radiation.

Absorption of longer-wave radiation by the atmosphere has the effect of warming the atmosphere. This is called the natural greenhouse effect. Water vapour (H_2O) and carbon dioxide (CO_2) are the main absorbing agents, together with ozone (O_3). The increase in the carbon dioxide content of the atmosphere over the last century, due to the burning of fossil fuels, is thought to enhance the greenhouse effect and to raise the temperature of the atmosphere above its natural level. This could have long-term climatic consequences. An image of part of Western Europe acquired by the Advanced Very High Resolution Radiometer (AVHRR) carried by the US NOAA-14 satellite is shown in Figure 1.12. The different colours show different levels of emitted thermal radiation in the 11.5 – 12.5 µm waveband. Before these colours can be interpreted in terms of temperatures, the effects of the atmosphere as well as the nature of the sensor calibration must be considered. Both these topics are covered in Chapter 4. For comparison, a visible band image of Europe and North Africa produced by the Meteosat-6 satellite is shown in Figure 1.13. Both images were collected by the UK NERC-funded satellite receiving station at Dundee University, Scotland. Both images were originally in greyscale but were converted to colour using a procedure called density slicing, which is considered in detail in Section 5.4.1.

That region of the spectrum composed of EMR with wavelengths between 1 mm and 300 cm is called the microwave band. Most satellite-borne sensors that operate in the microwave region use microwave radiation

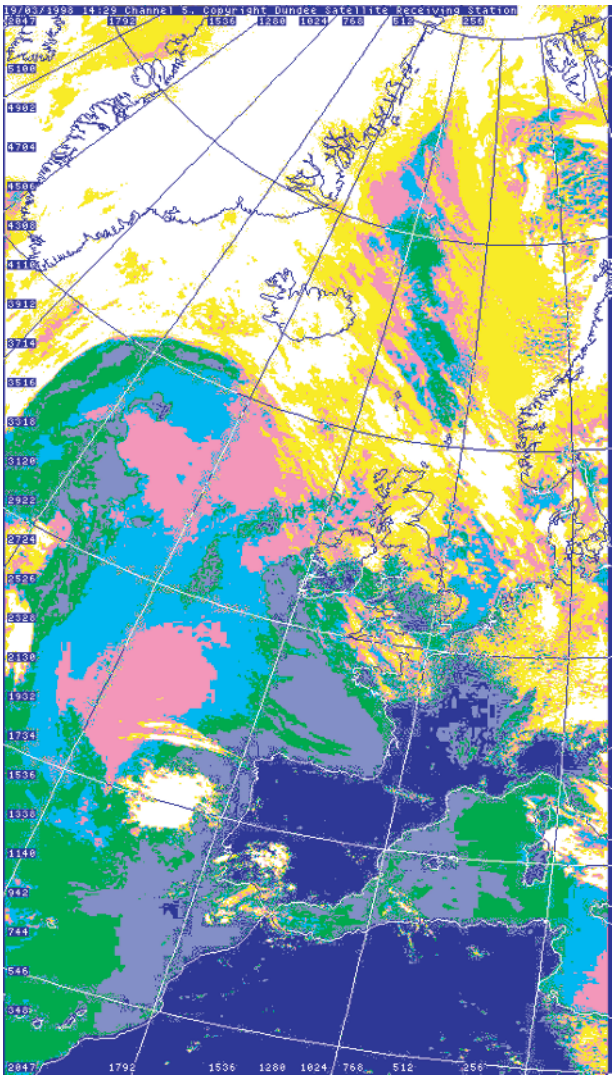

Figure 1.12 *NOAA AVHRR band 5 image (thermal infrared, 11.5–12.5 µm) of western Europe and NW Africa collected at 14.20 on 19 March 1998. The image was downloaded by the NERC Satellite Receiving Station at Dundee University, UK, where the image was geometrically rectified (Chapter 4) and the latitude/longitude grid and digital coastline were added. Darker colours (dark blue, dark green) areas indicate greater thermal emissions. The position of a high-pressure area (anti-cyclone) can be inferred from cloud patterns. Cloud tops are cold and therefore appear white. The NOAA satellite took just over 15 minutes to travel from the south to the north of the area shown on this image. The colour sequence is (from cold to warm): dark blue–dark green–green–light cyan–pink–yellow–white. © Dundee Satellite Receiving Station, Dundee University.*

with wavelengths between 3 and 25 cm. Radiation at these wavelengths can penetrate cloud, and the microwave band is thus a valuable region for remote sensing in temperate and tropical areas where cloud cover restricts the collection of optical and TIR images.

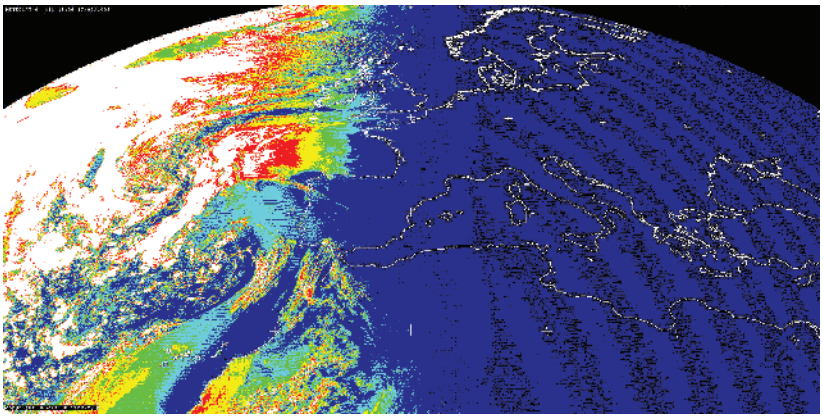

Figure 1.13 *Portion of a Meteosat-6 visible channel image of Europe and North Africa taken at 18.00 on 17 March 1998, when the lights were going on across Europe. Image received by Dundee University, UK. The colour sequence is black–dark blue–cyan–green–yellow–red–white. The banding pattern on the right side of the image (black stripes) is probably electronic noise.* © *Dundee Satellite Receiving Station, Dundee University.*

Some microwave sensors can detect the small amounts of radiation at these wavelengths that is emitted by the Earth. Such sensors are called passive because they detect EMR that is generated externally, for example by emittance by or reflectance from a target. Passive microwave radiometers such as the SMMR (scanning multichannel microwave radiometer) produce imagery with a low spatial resolution (Section 2.2.1) that is used to provide measurements of sea-surface temperature and wind speed, and also to detect sea ice.

Because the level of microwave energy emitted by the Earth is very low, a high-resolution imaging microwave sensor generates its own EMR at centimetre wavelengths, transmits this energy towards the ground and then detects the strength of the return signal that is scattered by the target in the direction of the sensor. Devices that generate their own electromagnetic energy are called *active* sensors to distinguish them from the *passive* sensors that are used to detect and record radiation of solar or terrestrial origin in the visible, IR and microwave wavebands. Thus, active microwave instruments are not dependent on an external source of radiation such as the Sun or, in the case of thermal emittance, the Earth. It follows that active microwave sensors can operate independently by day or by night. An analogy that is often used is that of a camera. In normal daylight, reflected radiation from the target enters the camera lens and exposes the film. Where illumination conditions are poor, the photographer employs a flashgun that generates radiation in visible wavebands, and the film is exposed by light from the flashgun that is reflected by the target. The microwave instrument produces pulses of energy, usually at centimetre wavelengths, that are transmitted by an antenna or aerial. The same antenna picks up the reflection of these energy pulses as they return from the target.

Microwave imaging sensors are called imaging radars (the word *radar* is an acronym, derived from *ra*dio *d*etection *a*nd *r*anging). The spatial resolution (Section 2.2.1) of imaging radars is a function of their antenna length. If a conventional ('brute force') radar is used, then antenna lengths become considerable as spatial resolution increases. Schreier (1993b, p. 107) notes that if the radar carried by the Seasat satellite (launched in 1981) had used a 'brute force' approach then its 10 m long antenna would have generated images with a spatial resolution of 20 km. A different approach, using several views of the target as the satellite approaches, reaches and passes the target, provides a means of achieving high resolution without the need for excessive antenna sizes. This approach uses the SAR principle, described in Section 2.4, and all satellite-borne radar systems have used the SAR principle. The main advantage of radar is that it is an all-weather, day–night, high spatial resolution instrument, which can operate independently of weather conditions or solar illumination. This makes it an ideal instrument for observing areas of the world such as the temperate and tropical regions, which are often cloud-covered and therefore inaccessible to optical and IR imaging sensors.

A radar signal does not detect either colour information (which is gained from analysis of optical wavelength sensors) or temperature information (derived from data collected by TIR sensors). It can detect both surface roughness and electrical conductivity information (which is related to soil moisture conditions). Because radar is an active rather than a passive instrument, the characteristics of the transmitted signal can be controlled. In particular, the wavelength, depression angle and polarisation of the signal are important properties of the radiation source used in remote sensing. Radar wavelength (Table 1.3)

Table 1.3 *Radar wavebands and nomenclature.*

Band designation	Frequency (MHz)	Wavelength (cm)
P	300–1000	30–100
L	1000–2000	15–30
S	2000–4000	7.5–15
C	4000–8000	3.75–7.5
X	8000–12 000	2.5–3.75
K_u	12 000–18 000	1.667–2.5
K	18 000–27 000	1.111–1.667
K_a	27 000–40 000	0.75–1.111

determines the observed roughness of the surface, in that a surface that has a roughness with a frequency less than that of the microwave radiation used by the radar is seen as smooth. An X-band (circa 3 cm wavelength) image of the area around the Richat structure in Mauretania is shown in Figure 1.14. Radar sensors are described in more detail in Section 2.4.

Beyond the microwave region is the radio band. Radio wavelengths are used in remote sensing, but not to detect Earth-surface phenomena. Commands sent to a satellite utilize radio wavelengths. Image data is transmitted to ground receiving stations using wavelengths in the microwave region of the spectrum; these data are recorded on the ground by high-speed tape-recorders while the satellite is in direct line of sight of a ground receiving station. Image data for regions of the world that are not within range of ground receiving stations are recorded by onboard tape-recorders or solid-state memory and these recorded data are subsequently transmitted together with currently scanned data when the satellite is within the reception range of a ground receiving station. The first three Landsat satellites (Section 2.3.6) used onboard tape recorders to supplement data that were directly transmitted to the ground. The latest Landsat (number 7) relies on the TDRS (Tracking and Data Relay Satellite) system, which allows direct broadcast of data from Earth resources satellites to one of a set of communications satellites located above the Equator in geostationary orbit (meaning that the satellite's orbital velocity is just sufficient to keep pace with the rotation of the Earth). The signal is relayed by the TDRS system to a ground receiving station at White Sands, NM, USA. European satellites use a similar system called Artemis, which became operational in 2003.

Figure 1.14 *X-band Synthetic aperture radar (SAR) image of the Richat geological structure in Mauretania collected by the Italian satellite COSMO-Skymed 1 on 8 October 2007. The structure is about 60 km in width. COSMO-Skymed (**CO**nstellation of small **S**atellites for **M**editerranean basin **O**bservation) plans to have five satellites in orbit eventually. The third was launched in October, 2008. (http://www.telespazio.it/GalleryMatera.html). COSMO-SkyMed Product © ASI-Agence Spatiale Italiana (YEAR) – All Rights Reserved.*

1.2.4 Sources of Electromagnetic Radiation

All objects whose temperature is greater than absolute zero, which is approximately −273 °C or 0 K (Kelvin), emit radiation. However, the distribution of the amount of radiation at each wavelength across the spectrum is not uniform. Radiation is emitted by the stars and planets; chief of these, as far as the human race is concerned, is the Sun, which provides the heat and light radiation needed to sustain life on Earth. The Sun is an almost-spherical body with a diameter of 1.39×10^6 km and a mean distance from Earth of 150×10^6 km. Its chief constituents are hydrogen and helium. The conversion of hydrogen to helium in the Sun's core provides the energy that is radiated from the outer layers. At the edge of the Earth's atmosphere the power received from the Sun, measured over the surface area of the Earth, is approximately 3.9×10^{22} MW which, if it were distributed evenly over the Earth, would give an incident radiant flux density of 1367 W m^{-2}. This value is known as the *solar constant*, even though it varies throughout the year by about ±3.5%, depending on the distance of the Earth from the Sun (and this variation is taken into account in the radiometric correction of remotely-sensed images; see Section 4.6). Bonhomme (1993) provides a useful summary of a number of aspects relating to solar radiation. On average, 35% of the incident radiant flux is reflected from the Earth (including clouds

and atmosphere), the atmosphere absorbs 17%, and 47% is absorbed by the materials forming the Earth's surface. From the Stefan–Boltzmann Law (below) it can be shown that the Sun's temperature is 5777 K if the solar constant is 1367 W m^{-2}. Other estimates of the Sun's temperature range from 5500 to 6200 K. The importance of establishing the surface temperature of the Sun lies in the fact that the distribution of energy emitted in the different regions of the electromagnetic spectrum depends upon the temperature of the source.

If the Sun were a perfect emitter, it would be an example of a theoretical ideal, called a *blackbody*. A blackbody transforms heat energy into radiant energy at the maximum rate that is consistent with the laws of thermodynamics (Suits, 1983). *Planck's Law* describes the spectral exitance (i.e. the distribution of radiant flux density with wavelength, Section 1.2.1) of a blackbody as:

$$M_\lambda = \frac{c_1}{\lambda^5(\exp[c_2/\lambda T] - 1)}$$

where

$c_1 = 3.742 \times 10^{-16}$ W m^{-2}
$c_2 = 1.4388 \times 10^{-2}$ m K
λ = wavelength (m)
T = temperature (Kelvin)
M_λ = spectral exitance per unit wavelength

Curves showing the spectral exitance of blackbodies at temperatures of 1000, 1600 and 2000 K are shown in Figure 1.15. The total radiant energy emitted by a blackbody is dependent on its temperature, and as temperature increases so the wavelength at which the maximum spectral exitance is achieved is reduced. The dotted line in Figure 1.15 joins the peaks of the spectral exitance curves. It is described by Wien's Displacement Law, which gives the wavelength of maximum spectral exitance (λ_m) in terms of temperature:

$$\lambda_m = \frac{c_3}{T}$$

and

$$c_3 = 2.898 \times 10^{-3} \text{ m K}$$

The total spectral exitance of a blackbody at temperature T is given by the Stefan–Boltzmann Law as:

$$M = \sigma T^4$$

In this equation, $\sigma = 5.6697 \times 10^{-8}$ W m^{-2} K^{-4}.

The distribution of the spectral exitance for a blackbody at 5900 K closely approximates the Sun's spectral exitance curve, while the Earth can be considered to act like a blackbody with a temperature of 290 K (Figure 1.16). The solar radiation maximum occurs in the visible spectrum, with maximum irradiance at 0.47 µm. About 46% of the total energy transmitted by the Sun falls into the visible waveband (0.4–0.76 µm).

Wavelength-dependent mechanisms of atmospheric absorption alter the actual amounts of solar irradiance that reach the surface of the Earth. Figure 1.17 shows the spectral irradiance from the Sun at the edge of the atmosphere (solid curve) and at the Earth's surface (broken line). Further discussion of absorption and scattering can be found in Section 1.2.5. The spectral distribution of radiant energy emitted by the Earth (Figure 1.16) peaks in the TIR wavebands at 9.7 µm. The amount of terrestrial emission is low in comparison with solar irradiance. However, the solar radiation absorbed by the atmosphere is balanced by terrestrial emission in the TIR, keeping the temperature of the atmosphere approximately constant. Furthermore, terrestrial TIR emission provides sufficient energy for remote sensing from orbital altitudes to be a practical proposition. The characteristics of the radiation sources used in remote sensing impose some limitations on the range of wavebands available for use. In general, remote sensing instruments that measure the spectral reflectance of solar

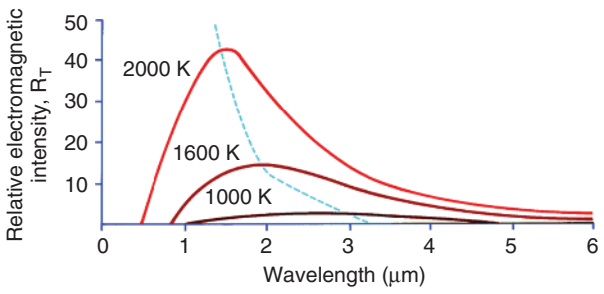

Figure 1.15 *Spectral exitance curves for blackbodies at temperatures of 1000, 1600 and 2000 K. The dotted line joins the emittance peaks of the curves and is described by Wien's Displacement Law (see text).*

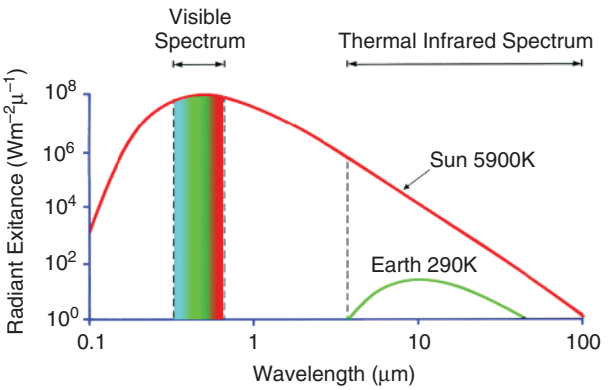

Figure 1.16 *Spectral exitance curves for blackbodies at 290 and 5900 K, the approximate temperatures of the Earth and the Sun.*

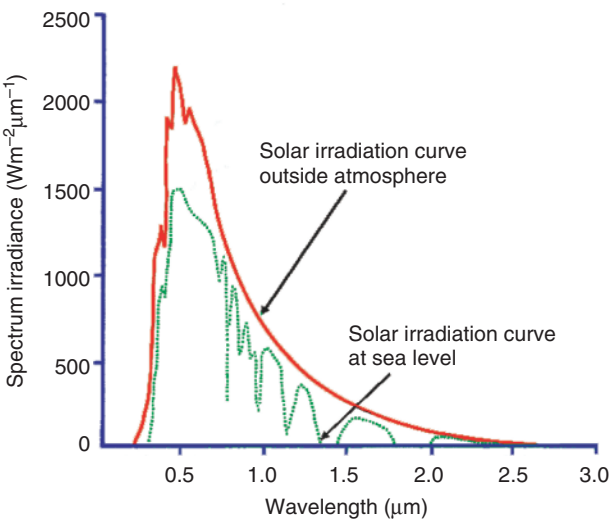

Figure 1.17 *Solar irradiance at the top of the atmosphere (solid line) and at sea-level (dotted line). Differences are due to atmospheric effects as discussed in the text. See also Figure 1.7.* Based on Manual of Remote Sensing, *Second Edition, ed. R.N. Colwell, 1983, Figure 5.5; Reproduced with permission from American Society for Photogrammetry and Remote Sensing, Manual of Remote Sensing.*

radiation from the Earth's surface are restricted to the wavelengths shorter than 2.5 μm. Instruments to detect terrestrial radiant exitance operate in the spectral region between 3 and 14 μm. Because of atmospheric absorption by carbon dioxide, ozone and water vapour, only the 3–5 and 8–14 μm regions of the TIR band are useful in remote sensing. An absorption band is also present in the 9–10 μm region. As noted earlier, the Earth's emittance peak occurs at 9.7 μm, so satellite-borne thermal sensors normally operate in the 10.5–12.5 μm spectral region. The 3–5 μm spectral window can be used to detect local targets that are hotter than their surroundings, for example forest fires. Since the 3–5 μm region also contains some reflected solar radiation it can only be used for temperature sensing at night.

Wien's Displacement Law (Figure 1.15) shows that the radiant power peak moves to shorter wavelengths as temperature increases, so that a forest fire will have a radiant energy peak at a wavelength shorter than 9.7 μm. Since targets such as forest fires are sporadic in nature and require high-resolution imagery the 3–5 μm spectral region is used by aircraft-mounted thermal detectors. This is a difficult region for remote sensing because it contains a mixture of reflected and emitted radiation, the effects of which are not easy to separate.

The selection of wavebands for use in remote sensing is therefore seen to be limited by several factors: primarily (i) the characteristics of the radiation source, as discussed in this section, (ii) the effects of atmospheric absorption and scattering (Section 1.2.5), and (iii) the nature of the target. This last point is considered in Section 1.3.

1.2.5 Interactions with the Earth's Atmosphere

In later chapters, we consider measurements of radiance from the Earth's surface made by instruments carried by satellites such as Landsat and SPOT that operate in the optical wavebands, that is, those parts of the electromagnetic spectrum with properties similar to those of visible light. It was noted at the beginning of this chapter that one aim of remote sensing is to identify the nature, and possibly the properties, of Earth surface materials from the spectral distribution of EMR that is reflected from, or emitted by, the target and recorded by the sensor. The existence of the atmosphere causes problems, because EMR from the Sun that is reflected by the Earth (the amount reflected depending on the reflectivity or albedo of the surface) and detected by the satellite or aircraft-borne sensor must pass through the atmosphere twice, once on its journey from the Sun to the Earth and once after being reflected by the surface of the Earth back to the sensor. During its passage through the atmosphere, EMR interacts with particulate matter suspended in the atmosphere and with the molecules of the constituent gases. This interaction is usually described in terms of two processes. One, called *scattering*, deflects the radiation from its path while the second process, *absorption*, converts the energy present in EMR into the internal energy of the absorbing molecule. Both absorption and scattering vary in their effect from one part of the spectrum to another. Remote sensing of the Earth's surface is impossible in those parts of the spectrum that are seriously affected by scattering and/or absorption, for these mechanisms effectively render the atmosphere opaque to incoming or outgoing radiation. As far as remote sensing of the Earth's surface is concerned, the atmosphere '. . . appears no other thing to me but a foul and pestilential congregation of vapours' (*Hamlet*, Act 2, Scene 2). Atmospheric absorption properties can, however, be useful. Remote sensing of the atmosphere uses these properties and a good example is the discovery and monitoring of the Antarctic ozone hole.

Regions of the spectrum that are relatively (but not completely) free from the effects of scattering and absorption are called *atmospheric windows;* EMR in these regions passes through the atmosphere with less modification than does radiation at other wavelengths (Figure 1.7). This effect can be compared to the way in which the bony tissues of the human body are opaque to X-rays, whereas the soft muscle tissue and blood are transparent. Similarly, glass is opaque to ultraviolet radiation but is transparent at the visible wavelengths. Figure 1.17 shows a plot of wavelength against the magnitude of incoming

radiation transmitted through the atmosphere; the window regions are those with a high transmittance. The same information is shown in a different way in Figure 1.7.

The effect of the processes of scattering and absorption is to add a degree of haze to the image, that is, to reduce the contrast of the image, and to reduce the amount of radiation returning to the sensor from the Earth's surface. A certain amount of radiation that is reflected from the neighbourhood of each target may also be recorded by the sensor as originating from the target. This is because scattering deflects the path taken by EMR as it travels through the atmosphere, while absorption involves the interception of photons or particles of radiation. Our eyes operate in the visible part of the spectrum by observing the light reflected by an object. The position of the object is deduced from the assumption that this light has travelled in a straight line between the object and our eyes. If some of the light reflected towards our eyes from the object is diverted from a straight path then the object will appear less bright. If light from other objects has been deflected so that it is apparently coming to our eyes from the direction of the first object then that first object will become blurred. Taken further, this scattering process will make it appear to our eyes that light is travelling from all target objects in a random fashion, and no objects will be distinguishable. Absorption reduces the amount of light that reaches our eyes, making a scene relatively duller. Both scattering and absorption, therefore, limit the usefulness of some portions of the electromagnetic spectrum for remote sensing purposes. They are known collectively as attenuation or extinction.

Scattering is the result of interactions between EMR and particles or gas molecules that are present in the atmosphere. These particles and molecules range in size from microscopic (with radii approximately equal to the wavelength of the EMR) to raindrop size (100 μm and larger). The effect of scattering is to redirect the incident radiation, or to deflect it from its path. The atmospheric gases that primarily cause scattering include oxygen, nitrogen and ozone. Their molecules have radii of less than 1 μm and affect EMR with wavelengths of 1 μm or less. Other types of particles reach the atmosphere both by natural causes (such as salt particles from oceanic evaporation or dust entrained by aeolian processes) or because of human activities (for instance, dust from soil erosion caused by poor land management practices, and smoke particles from industrial and domestic pollution). Some particles are generated by photochemical reactions involving trace gases such as sulfur dioxide or hydrogen sulfide. The former may reach the atmosphere from car exhausts or from the combustion of fossil fuels. Another type of particle is the raindrop, which tends to be larger than the other kinds of particles mentioned previously (10–100 μm compared to 0.1–10 μm radius). The concentration of particulate matter varies both in time and over space. Human activities, particularly agriculture and industry, are not evenly spread throughout the world, nor are natural processes such as wind erosion or volcanic activity. Meteorological factors cause variations in atmospheric turbidity over time, as well as over space. Thus, the effects of scattering are spatially uneven (the degree of variation depending on weather conditions) and vary from time to time. Remotely-sensed images of a particular area will thus be subjected to different degrees of atmospheric scattering on each occasion that they are produced. Differences in atmospheric conditions over time are the cause of considerable difficulty in the quantitative analysis of time sequences of remotely-sensed images.

The mechanisms of scattering are complex, and are beyond the scope of this book. However, it is possible to make a simple distinction between selective and non-selective scattering. Selective scattering affects specific wavelengths of EMR, while non-selective scattering is wavelength independent. Very small particles and molecules, with radii far less than the wavelength of the EMR of interest, are responsible for *Rayleigh scattering*. The effect of this type of scattering is inversely proportional to the fourth power of the wavelength, which implies that shorter wavelengths are much more seriously affected than longer wavelengths. Blue light (wavelength 0.4–0.5 μm) is thus more powerfully scattered than red light (0.6–0.7 μm). This is why the sky seems blue, for incoming blue light is so scattered by the atmosphere that it seems to reach our eyes from all directions, whereas at the red end of the visible spectrum scattering is much less significant so that red light maintains its directional properties. The sky appears to be much darker blue when seen from a high altitude, such as from the top of a mountain or from an aeroplane, because the degree of scattering is reduced due to the reduction in the length of the path traversed through the atmosphere by the incoming solar radiation. Scattered light reaching the Earth's surface is termed diffuse (as opposed to *direct*) irradiance or, more simply, *skylight*. Radiation that has been scattered within the atmosphere and which reaches the sensor without having made contact with the Earth's surface is called the *atmospheric path radiance*.

Mie scattering is caused by particles that have radii between 0.1 and 10 μm, that is approximately the same magnitude as the wavelengths of EMR in the visible, NIR and TIR regions of the spectrum. Particles of smoke, dust and salt have radii of these dimensions. The intensity of Mie scattering is inversely proportional to wavelength, as in the case of Rayleigh scattering. However, the exponent ranges in value from -0.7 to -2 rather than the -4 of Rayleigh scattering. Mie scattering affects shorter wavelengths more than longer wavelengths, but the disparity is not as great as in the case of Rayleigh scattering.

Non-selective scattering is wavelength-independent. It is produced by particles whose radii exceed 10 µm. Such particles include water droplets and ice fragments present in clouds. All visible wavelengths are scattered by such particles. We cannot see through clouds because all visible wavelengths are non-selectively scattered by the water droplets of which the cloud is formed. The effect of scattering is, as mentioned earlier, to increase the haze level or reduce the contrast in an image. If contrast is defined as the ratio between the brightest and darkest areas of an image, and if brightness is measured on a scale running from 0 (darkest) to 100 (brightest), then a given image with a brightest area of 90 and a darkest area of 10 will have a contrast of 9. If scattering has the effect of adding a component of upwelling radiation of 10 units then the contrast becomes 100 : 20 or 5. This reduction in contrast will result in a decrease in the detectability of features present in the image. Figure 1.18 shows relative scatter as a function of wavelength for the 0.3–1.0 µm region of the spectrum for a variety of levels of atmospheric haze.

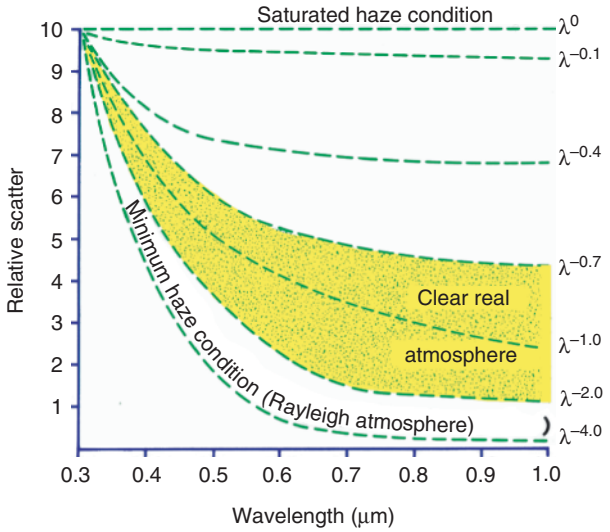

Figure 1.18 *Relative scatter as a function of wavelength for a range of atmospheric haze conditions. Based on R.N. Colwell (ed.), 1983,* Manual of Remote Sensing*, Second Edition, Figure 6.15. Reproduced with permission from American Society for Photogrammetry and Remote Sensing, Manual of Remote Sensing.*

Absorption is the second process by which the Earth's atmosphere interacts with incoming EMR. Gases such as water vapour, carbon dioxide and ozone absorb radiation in particular, regions of the electromagnetic spectrum called absorption bands. The processes involved are very complex and are related to the vibrational and rotational properties of the molecules of water vapour, carbon dioxide or ozone, and are caused by transitions in the energy levels of the atoms. These transitions occur at characteristic wavelengths for each type of atom and at these wavelengths absorption rather than scattering is dominant. Remote sensing in these absorption bands is thus rendered impossible. Fortunately, other regions of the spectrum with low absorption (high transmission) can be used. These regions are called 'windows', and they cover the 0.3–1.3 µm (visible/NIR), 1.5–1.8, 2.0–2.5 and 3.5–4.1 µm (middle IR) and 7.0–15.0 µm (TIR) wavebands. The utility of these regions of the electromagnetic spectrum in remote sensing is considered at a later stage.

1.3 Interaction with Earth-Surface Materials

1.3.1 Introduction

Electromagnetic energy reaching the Earth's surface from the Sun is reflected, transmitted or absorbed. Reflected energy travels upwards through, and interacts with, the atmosphere; that part of it which enters the field of view of the sensor (Section 2.2.1) is detected and converted into a numerical value that is transmitted to a ground receiving station on Earth. The amount and spectral distribution of the reflected energy is used in remote sensing to infer the nature of the reflecting surface. A basic assumption made in remote sensing is that specific targets (soils of different types, water with varying degrees of impurities, rocks of differing lithologies or vegetation of various species) have an individual and characteristic manner of interacting with incident radiation that is described by the spectral response of that target. In some instances, the nature of the interaction between incident radiation and Earth-surface material will vary from time to time during the year, such as might be expected in the case of vegetation as it develops from the leafing stage, through growth to maturity and, finally, to senescence.

The spectral response of a target also depends upon such factors as the orientation of the Sun (solar azimuth, Figure 1.19), the height of the Sun in the sky (solar elevation angle), the direction that the sensor is pointing relative to nadir (the look angle) and the state of health of vegetation, if that is the target. Nevertheless, if the assumption that specific targets are characterized by an individual spectral response were invalid then Earth Observation (EO) by remote sensing would be an impossible task. Fortunately, experimental studies in the field and in the laboratory, as well as experience with multispectral imagery, have shown that the assumption is generally a reasonable one. Indeed, the successful development of remote sensing of the environment over the last few decades bears witness to its validity. Note that the term *spectral signature* is sometimes used to describe the spectral response curve for a target. In view of the dependence of spectral response on the factors mentioned above, this term is inappropriate for

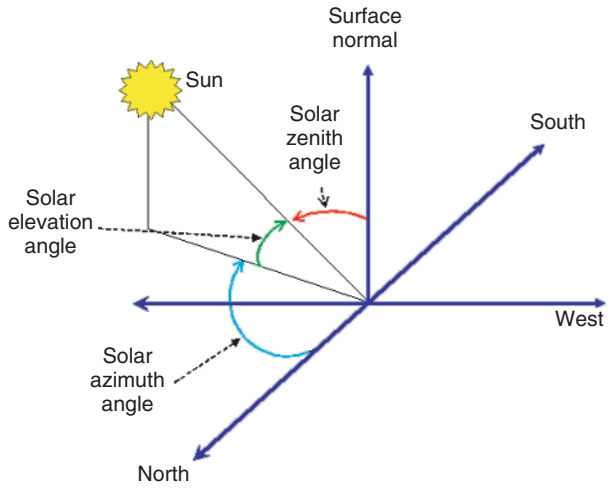

Figure 1.19 *Solar elevation and azimuth angles. The elevation angle of the Sun – target line is measured upwards from the horizontal plane. The zenith angle is measured from the surface normal, and is equal to (90 – elevation angle)°. Azimuth is measured clockwise from north.*

it gives a misleading impression of constancy. Remote sensing scientists are not alone in trying to estimate the nature of surface materials from their spectral reflection properties; an English newspaper, the *Daily Telegraph* (16 March 2009), reported that a thief routinely used Google Earth to identify and steal lead sheathing on the roofs of churches and public buildings.

In this section, spectral reflectance curves of vegetation, soil, rocks and water are examined in order to emphasize their characteristic features. The results summarized in the following paragraphs must not be taken to be characteristic of all varieties of materials or all observational circumstances. One of the problems met in remote sensing is that the spectral reflectance of a given Earth-surface cover type is influenced by a variety of confusing factors. For example, the spectral reflectance curve of a particular agricultural crop such as wheat is not constant over time, nor is it the same for all kinds of wheat. The spectral reflectance curve is affected by factors such as soil nutrient status, the growth stage of the vegetation, the colour of the soil (which may be affected by recent weather conditions), the solar azimuth and elevation angles and the look angle of the sensor. The topographic position of the target in terms of slope orientation with respect to solar azimuth and slope angle also has an effect on the reflectance characteristics of the target, as will the state of the atmosphere. Methods for dealing with some of these difficulties are described in Sections 4.5 and 4.7. Hence, the examples given in this section are idealized models rather than templates.

Before turning to the individual spectral reflectance features of Earth surface materials, a distinction must be drawn between two kinds of reflectance that occur at a surface. *Specular* reflection is that kind of reflection in which energy leaves the reflecting surface without being scattered, with the angle of incidence being equal to the angle of reflectance (Figure 1.4a). Surfaces that reflect *specularly* are smooth relative to the wavelength of the incident energy. *Diffuse* or Lambertian reflectance occurs when the reflecting surface is rough relative to the wavelength of the incident energy, and the incident energy is scattered in all directions (Figure 1.4b). A mirror reflects specularly while a piece of paper reflects diffusely. In the visible part of the spectrum, many terrestrial targets are diffuse reflectors, whereas calm water can act as a specular reflector. At microwave wavelengths, however, some terrestrial targets are specular reflectors, while volume reflectance (scattering) can occur at optical wavelengths in the atmosphere and the oceans, and at microwave wavelengths in vegetation (Figure 1.4d).

A satellite sensor operating in the visible and NIR spectral regions does not detect all the reflected energy from a ground target over an entire hemisphere. It records the reflected energy that is returned at a particular angle (see the definition of radiance in Section 1.2.1). To make use of these measurements, the distribution of radiance at all possible observation and illumination angles (called the *bidirectional reflectance distribution function*; BRDF) must be taken into consideration. Details of the BRDF are given by Slater (1980) who writes:

> . . .the reflectance of a surface depends on both the direction of the irradiating flux and the direction along which the reflected flux is detected.

Hyman and Barnsley (1997) demonstrate that multiple images of the same area taken at different viewing angles provide enough information to allow different land cover types to be identified as a result of their differing BRDF. The MISR (Multi-Angle Imaging SpectroRadiometer) instrument, carried by the American Terra satellite, collects multi-directional observations of the same ground area over a timescale of a few minutes, at nadir and at fore and aft angles of view of 21.1°, 45.6°, 60.0° and 70.5° and in four spectral bands in the visible and NIR regions of the electromagnetic spectrum. The instrument therefore provides data for the analysis and characterisation of reflectance variation of Earth surface materials over a range of angles (Diner *et al*., 1991). Chopping *et al*. (2003) use a BRDF model to extract information on vegetation canopy physiognomy. The European Space Agency's (ESA's) Compact High Resolution Imaging Spectrometer (CHRIS), carried by a small satellite named PROBA (Project for On Board Autonomy) can image an 18.6 km^2 area with its high resolution mode at multiple angles. See http://directory.eoportal.org/get_announce.php?an_id=7299. Furthermore, its agile

platform can be tilted during acquisition so multi-angle observations can be acquired. See Guanter, Alonso and Moreno (2005) for more details of the PROBA/CHRIS mission and its first results.

It follows from the foregoing that, even if the target is a diffuse reflector such that incident radiation is scattered in all directions, the assumption that radiance is constant for any observation angle θ measured from the surface normal does not generally hold. A simplifying assumption is known as *Lambert's Cosine Law*, which states that the radiance measured at an observation angle θ is the same as that measured at an observation angle of 0° adjusted for the fact that the projection of the unit surface at a view angle of θ is proportional to $\cos\theta$ (Figure 1.20). Surfaces exhibiting this property are called 'Lambertian', and a considerable body of work in remote sensing either explicitly or implicitly assumes that Lambert's Law applies. However, it is usually the case that the spectral distribution of reflected flux from a surface is more complex than the simple description provided by Lambert's Law, for it depends on the geometrical conditions of measurement and illumination. The topic of correction of images for sun and view angle effects is considered further in Chapter 4.

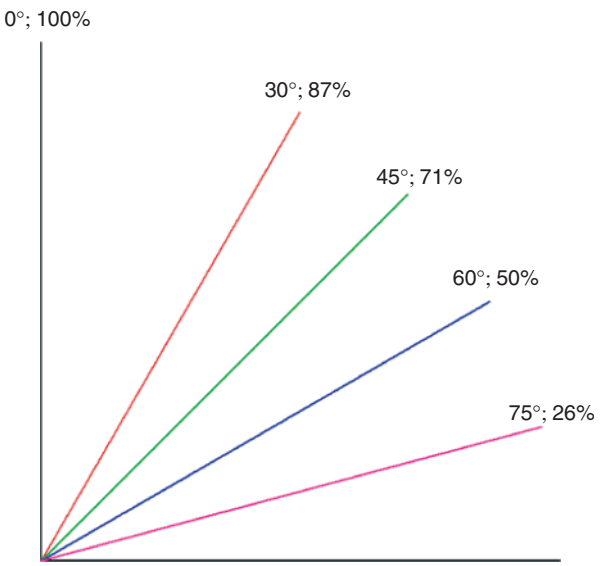

Figure 1.20 *Lambert's cosine law. Assume that the illumination angle is 0°. A range of view angles is shown, together with the percentage of incoming radiance that is scattered in the direction of the view angle.*

1.3.2 Spectral Reflectance of Earth Surface Materials

In this section, typical spectral reflectance curves for characteristic types of Earth-surface materials are discussed. The remarks in Section 1.3.1 should not be overlooked when reading the following paragraphs. The Earth-surface materials that are considered in this section are vegetation, soil, bare rock and water. The short review by Verstraete and Pinty (1992) is recommended. Hobbs and Mooney (1990) provide a useful survey of remote sensing of the biosphere. Aplin (2004, 2005) covers progress in remote sensing in ecology.

1.3.2.1 Vegetation

The reflectance spectra of 3 pixels selected from a DAIS imaging spectrometer data set (Section 9.3) covering a small area of La Mancha in central Spain (Figure 1.21a) show that real-world vegetation spectra conform to the ideal pattern, though there is significant variation, especially in the NIR region. Two of the three curves in Figure 1.21b show relatively low values in the red and the blue regions of the visible spectrum, with a minor peak in the green region. These peaks and troughs are caused by absorption of blue and red light by chlorophyll and other pigments. Typically, 70–90% of blue and red light is absorbed to provide energy for the process of photosynthesis. The slight reflectance peak in the green waveband between 0.5 and 0.6 µm is the reason that actively growing vegetation appears green to the human eye. Non-photosynthetically active vegetation lacks this 'green peak'.

For photosynthetically active vegetation, the spectral reflectance curve rises sharply between about 0.65 and 0.76 µm, and remains high in the NIR region between 0.75 and 1.35 µm because of interactions between the internal leaf structure and EMR at these wavelengths. Internal leaf structure has some effect between 1.35 and 2.5 µm, but reflectance is largely controlled by leaf-tissue water content, which is the cause of the minima recorded near 1.45 and 1.95 µm. The status of the vegetation (in terms of photosynthetic activity) is frequently characterized by the position of a point representative of the steep rise in reflectance at around 0.7 µm. This point is called the red edge point, and its characterization and uses are considered in Section 9.3.2.3.

As the plant senesces, the level of reflectance in the NIR region (0.75–1.35 µm) declines first, with reflectance in the visible part of the spectrum not being affected significantly. This effect is demonstrated by the reflectance spectrum shown in orange on Figure 1.21. The slope of the curve from the red to the NIR region of the spectrum is lower, as is the reflectance in the area of the 'infrared plateau'. However, changes in reflectance in the visible region are not so apparent. As senescence continues, the relative maximum in the green part of the visible spectrum declines as pigments other than chlorophyll begin to dominate, and the leaf begins to lose its greenness and to turn yellow or reddish, depending on species. The

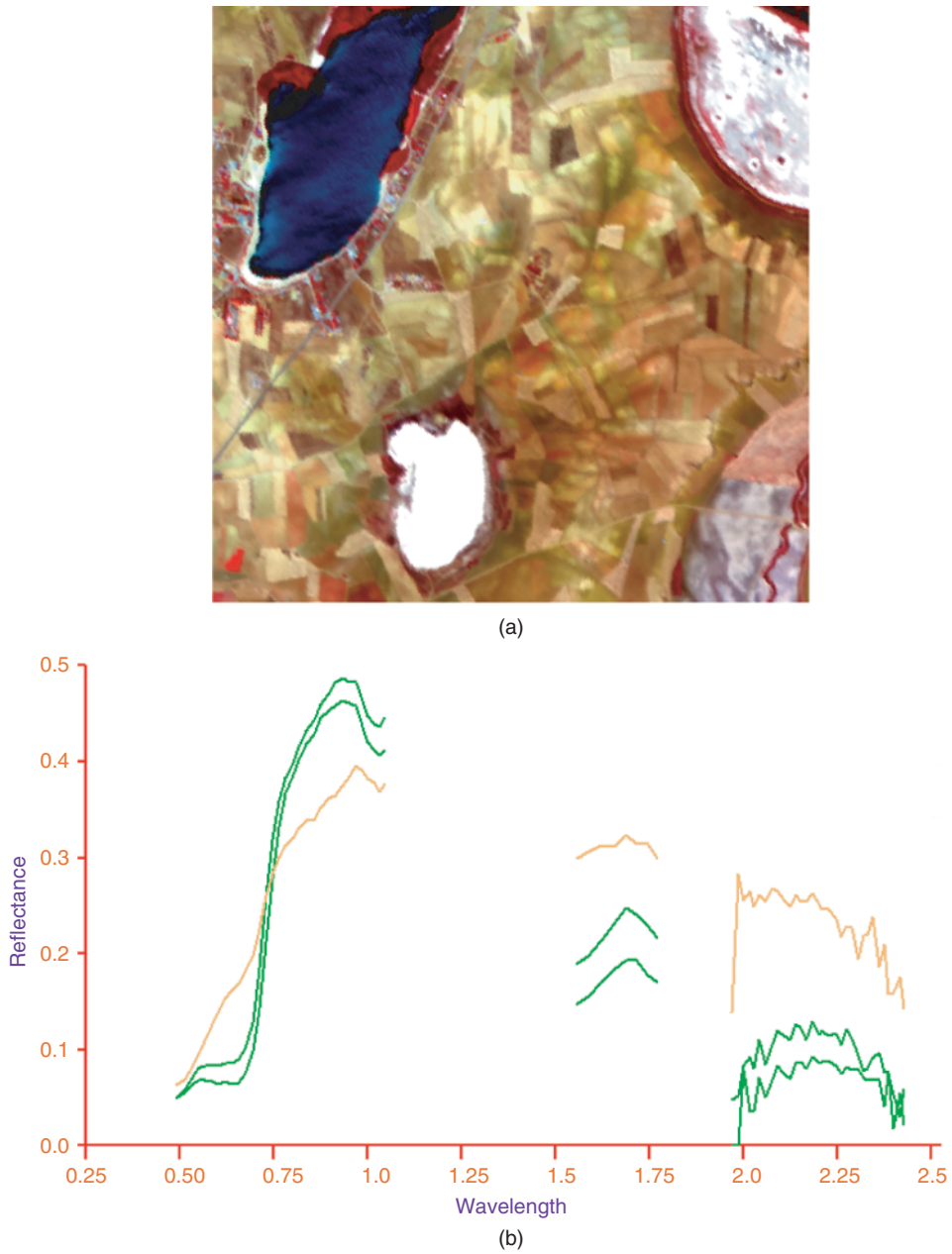

Figure 1.21 *(a) DAIS image of part of La Mancha, Central Spain. (b) Reflectance spectra in the optical wavebands of three vegetation pixels selected from this image. The two green curves represent the typical spectral reflectance curves of active vegetation. The 2 pixels which these curves represent were selected from the bright red area in the bottom left of image (a) and the similar area by the side of the black lagoon. The third reflectance curve, shown in orange, was selected from the orange area in the top right of image (a). The spectral reflectance plots are discontinuous because parts of the atmosphere absorb and/or scatter incoming and outgoing radiation (see Figure 1.7 and Chapter 4). Reproduced with permission from the German Space Agency, DLR.*

wavelength of the red edge point also changes. Stress caused by environmental factors such as drought or by the presence or absence of particular minerals in the soil can also produce a spectral response that is similar to senescence. Areas of vegetation showing adverse effects due to the presence (or absence) of certain minerals in the soil are called geobotanical anomalies, and their distribution has been used successfully to determine the location of mineral deposits (Goetz, Rock and Rowan, 1983).

The shape of the spectral reflectance curve is used to distinguish vegetated and non-vegetated areas on remotely-sensed imagery. Differences between species can also be

considerable, and may be sufficient to permit their discrimination, depending on the number, width and location of the wavebands used by the sensor (Section 2.2). Such discrimination may be possible on the basis of relative differences in the spectral reflectance curves of the vegetation or crop types. Absolute reflectance values (Section 4.6) may be used to estimate physical properties of the vegetation, such as leaf area index (LAI) or biomass production. In agriculture, the estimation of crop yields is often a significant economic requirement. Ratios of reflectance values in two or more spectral bands are widely used to characterize vegetation (Section 6.2.4). It is important to remember, however, the points made in Section 1.3.1; there is no single, ideal spectral reflectance curve for any particular vegetation type, and the recorded radiance from a point on the ground will depend upon the viewing and illumination angles, as well as other variables. The geometry of the crop canopy will strongly influence the BRDF (Section 1.3.1), while factors such as the transmittance of the leaves, the number of leaf layers, the actual arrangement of leaves on the plant and the nature of the background (which may be soil, or leaf litter or undergrowth) are also important. In order to distinguish between some types of vegetation, and to assess growth rates from remotely-sensed imagery, it is necessary to use *multi-temporal imagery*, that is imagery of the same area collected at different periods in the growing season.

1.3.2.2 Geology

Geological use of remotely-sensed imagery relies, to some extent, upon knowledge of the spectral reflectance curves of vegetation, for approximately 70% of the Earth's land surface is vegetated and the underlying rocks cannot be observed directly, and differences in soil and underlying bedrock can be seen in the distribution of vegetation species, numbers of species and vigour. Even in the absence of vegetated surfaces, weathering products generally cover the bedrock. It was noted in the preceding section that geobotanical anomalies might be used to infer the location of mineral deposits. Such anomalies include peculiar or unexpected species distribution, stunted growth or reduced ground cover, altered leaf pigmentation or yellowing (chlorosis) and alteration to the phenological cycle, such as early senescence or late leafing in the spring. It would be unwise to suggest that all such changes are due to soil geochemistry; however, the results of a number of studies indicate that the identification of anomalies in the vegetation cover of an area can be used as a guide to the presence of mineral deposits. If the relationship between soil formation and underlying lithology has been destroyed, for example by the deposition of glacial material over the local rock, then it becomes difficult to make associations between the phenological characteristics of the vegetation and lithology of the underlying rocks.

In semi-arid and arid areas such as the Great Sandy Desert of Western Australia (Figure 1.22), the spectral reflectance curves of rocks and minerals may be used directly in order to infer the lithology of the study area, though care should be taken because weathering crusts with spectra that are significantly different from the parent rock may develop. Laboratory studies of reflectance spectra of minerals have been carried out by Hunt and co-workers in the United States (Hunt, 1977, 1979; Hunt and Ashley, 1979; Hunt and Salisbury, 1970, 1971; Hunt, Salisbury and Lenhoff, 1971). Spectral libraries, accessible over the Internet from the Jet Propulsion Laboratory (the ASTER Spectral Library and the US Geological Survey Digital Spectral Library), contain downloadable data derived from the studies of Hunt, Salisbury and others. A new version (numbered 2.0) of the ASTER Spectral Library is now available (Baldridge *et al*., 2009) and can be found at http://speclib.jpl.nasa.gov/. These studies demonstrate that rock-forming minerals have unique

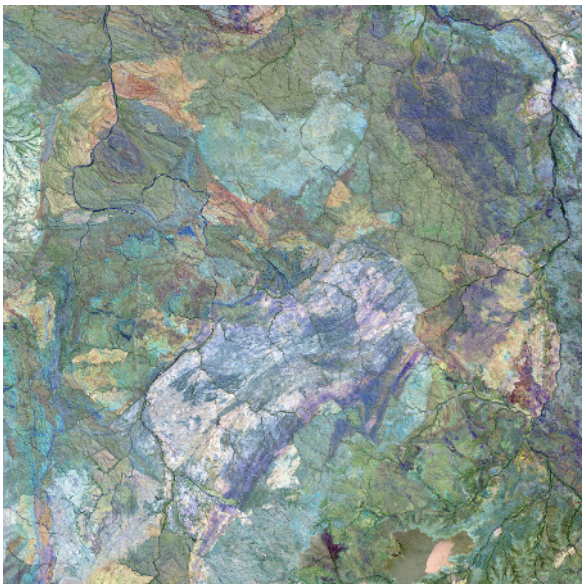

Figure 1.22 *Landsat-7 Thematic Mapper image of the Great Sandy Desert of Western Australia. Despite its name, not all of the desert is sandy and this image shows how the differing spectral reflectance properties of the weathered rock surfaces allow rock types to be differentiated. Field work would be necessary to identify the specific rock types, while comparison of the spectral reflectance properties at each pixel with library spectra (such as those contained in the ASTER spectral library, for example Figure 1.23) may allow the identification of specific minerals. The image was collected on 24 February 2001 and was made using shortwave-infrared, near-infrared and red wavelengths as the red, green and blue components of this false-colour composite image. Image courtesy NASA/USGS.*

spectral reflectance curves. The presence of absorption features in these curves is diagnostic of the presence of certain mineral types. Some minerals, for example quartz and feldspars, do not have strong absorption features in the visible and NIR regions, but can be important as dilutants for minerals with strong spectral features such as the clay minerals, sulfates and carbonates. Clay minerals have a decreasing spectral reflectance beyond 1.6 μm, while carbonate and silicate mineralogy can be inferred from the presence of absorption bands in the mid-IR region, particularly 2.0–2.5 μm. Kahle and Rowan (1980) show that multi-spectral TIR imagery in the 8–12 μm region can be used to distinguish silicate and non-silicate rocks. Two examples of library spectra (for limestone and basalt) are shown in Figure 1.23. The data for these figures were derived from the ASTER Spectral Library.

Some of the difficulties involved in the identification of rocks and minerals from the properties of spectral reflectance curves include the effects of atmospheric scattering and absorption, the solar flux levels in the spectral regions of interest (Section 1.2.5) and the effects of weathering. Buckingham and Sommer (1983) indicate

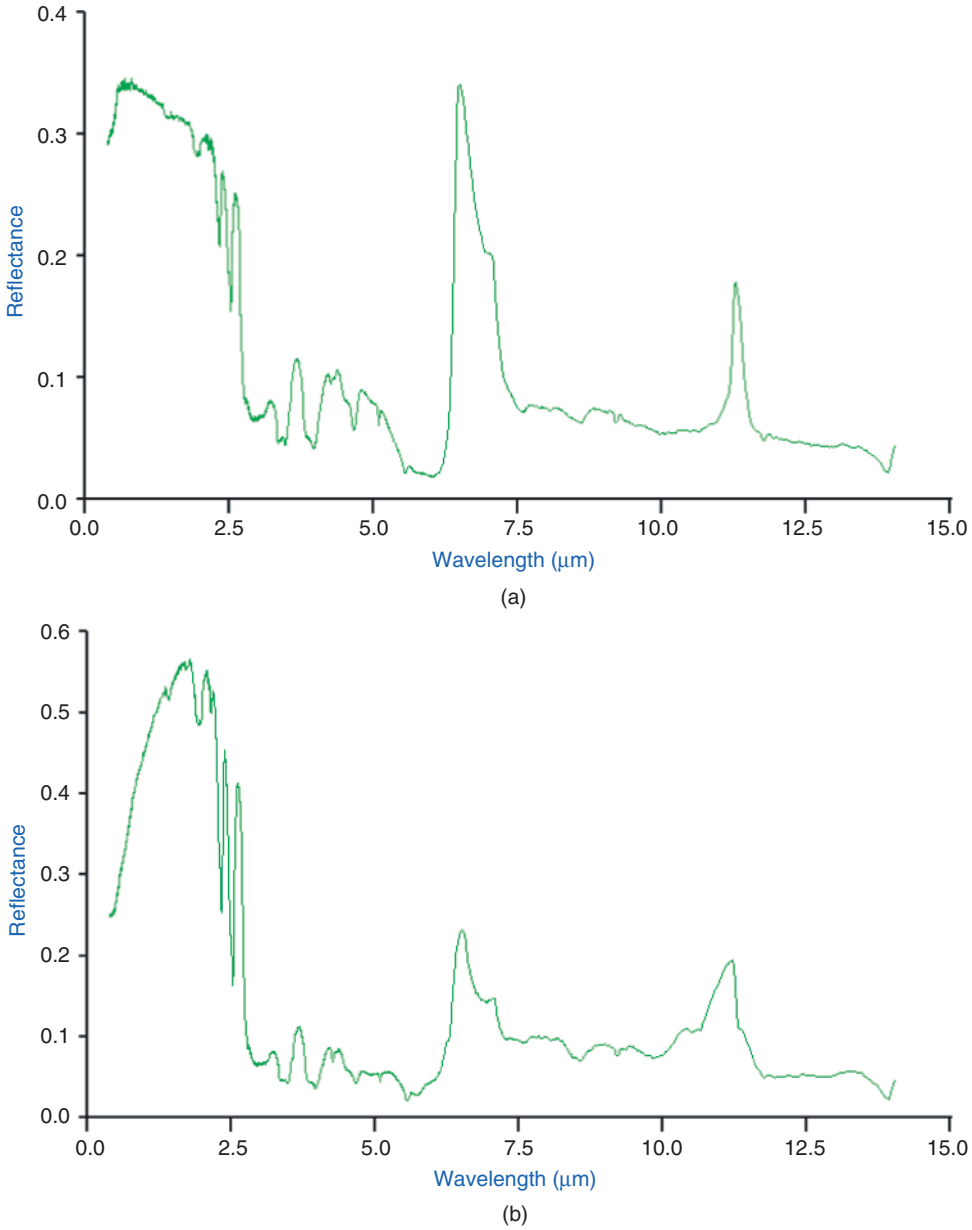

Figure 1.23 *Reflectance and emittance spectra of (a) limestone and (b) basalt samples. Data from the ASTER spectral library through the courtesy the Jet Propulsion Laboratory, California Institute of Technology,Pasadena, California,*

that the nature of the spectral reflectance of a rock is determined by the mineralogy of the upper 50 μm, and that weathering, which produces a surface layer that is different in composition from the parent rock, can significantly alter the observed spectral reflectance.

The use of multiband (or hyperspectral) imaging spectrometers mounted on aircraft and satellites can now measure the spectra of ground surface materials at a large number of closely spaced points. The interpretation of these spectra requires a detailed knowledge of the chemistry of the materials concerned. Imaging spectrometers are described in Chapter 9. Clark (1999) gives an accessible survey of the use of imaging spectrometers in identifying surface materials. Introductions to geological remote sensing are Drury (2004), Goetz (1989), Gupta (2003), Prost (2002) and Vincent (1997).

1.3.2.3 Water Bodies

The characteristic spectral reflectance curve for water shows a general reduction in reflectance with increasing wavelength in the visible wavebands, so that in the NIR the reflectance of deep, clear water is virtually zero. This is shown schematically in Figure 1.24a, in which the penetration depth of red, green and blue light is indicated by the arrows depicted in those colours. The black arrow represents NIR radiation, which is absorbed by the first few centimetres of water. Figure 1.25 shows an image of the Tanzanian coast south of Dar-es-Salaam. The red component of the

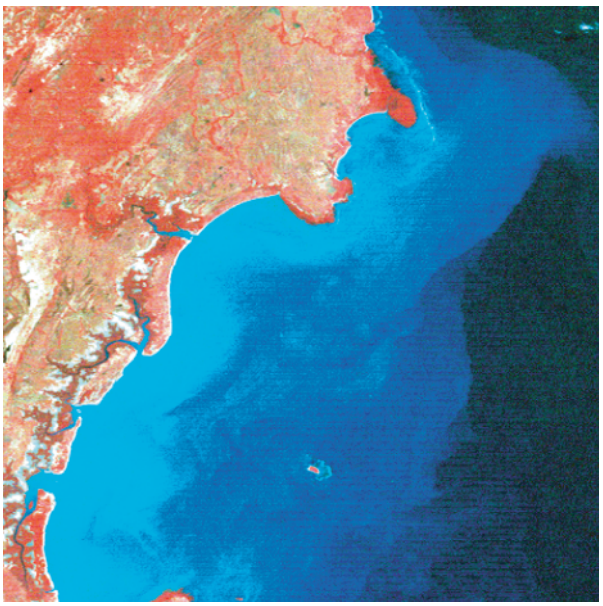

Figure 1.25 *Image of the coast of Tanzania south of Dar-es-Salaam. Shades of red in the image show spatial variations in near-infrared reflectance, while shades of green in the image show variations in the reflectance of red light. Blue shades in the image show variations in the reflectance of green light. This representation is usually termed 'false colour'. Black shows no reflection in any of the three wavebands, whereas lighter colours show higher reflectance. The water in this area is clear and the reflection from the sea bed is visible, showing the extent of the continental shelf. This image was taken by Landsat's Multispectral Scanner (MSS), which is described in Chapter 2. Image courtesy of NASA/USGS.*

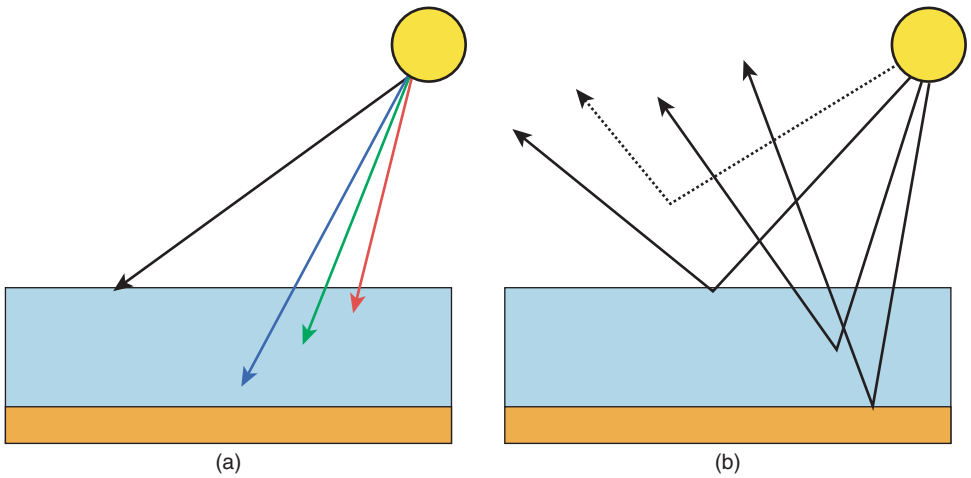

Figure 1.24 *(a) Showing the differential penetration depths of red, green and blue light in clear, calm water. The black line shows longer (infrared) wavelengths that are totally absorbed by the first few centimetres of water. (b) The solid arrows show, from right to left, bottom reflectance (the water depth is assumed to be less than the depth of penetration of blue light), volume reflectance (caused by light being scattered by suspended sediment particles, phytoplankton, dissolved organic matter and surface reflectance. The dotted line shows the path taken by light from the Sun that interacts with the atmosphere in the process of atmospheric scattering (Chapter 4). Electromagnetic radiation scattered by the atmosphere may be considerably greater in magnitude than that which is backscattered by surface reflectance, volume reflectance and bottom reflectance.*

image shows variations in the NIR reflectance of the land and water surface, the green component of the image shows variations in visible red reflectance and the blue component of the image shows variations in the visible green reflectance. The increase in reflection from the water from the deep, offshore region (where the ocean is seen as black) to the inshore region, where the colour changes to blue then blue–green, is clearly apparent. The edge of the continental shelf is shown as an abrupt change of colour, from light blue to black. The red colour of the land surface shows the presence of vegetation, which reflects strongly in the NIR, as noted in Section 1.3.2.1.

The spectral reflectance of water is affected by the presence and concentration of dissolved and suspended organic and inorganic material, and by the depth of the water body. Thus, the intensity and distribution of the radiance upwelling from a water body are indicative of the nature of the dissolved and suspended matter in the water, and of the water depth. Figure 1.24b shows how the information that oceanographers and hydrologists require is only a part of the total signal received at the sensor. Solar irradiance is partially scattered by the atmosphere, and some of this scattered light (the path radiance) reaches the sensor. Next, part of the surviving irradiance is reflected by the surface of the water body. This reflection might be specular under calm conditions, or its distribution might be strongly influenced by surface waves and the position of the sun relative to the sensor, giving rise to *sunglint*. Once within the water body, EMR may be absorbed by the water (the degree of absorption being strongly wavelength-dependent) or selectively absorbed by dissolved substances, or back-scattered by suspended particles. This latter component is termed the volume reflectance. At a depth of 20 m only visible light (mainly in the blue region) is present, as the NIR component has been completely absorbed. Particulate matter, or suspended solids, scatters the downwelling radiation, the degree of scatter being proportional to the concentration of particulates, although other factors such as the particle-size distribution and the colour of the sediment are significant. Over much of the observed low to medium range of concentrations of suspended matter a positive, linear relationship between suspended matter concentration and reflectance in the visible and NIR bands has been observed, though the relationship becomes non-linear at increasing concentrations. Furthermore, the peak of the reflectance curve moves to progressively longer wavelengths as concentration increases, which may lead to inaccuracy in the estimation of concentration levels of suspended materials in surface waters from remotely-sensed data. Another source of error is the inhomogeneous distribution of suspended matter through the water body, which is termed *patchiness*.

The presence of chlorophyll is an indication of the trophic status of lakes and is also of importance in estimating the level of organic matter in coastal and estuarine environments. Whereas suspended matter has a generally broadband reflectance in the visible and NIR, chlorophyll exhibits absorption bands in the region below 0.5 µm and between 0.64 and 0.69 µm. Detection of the presence of chlorophyll therefore requires an instrument with a higher spectral resolution (Section 2.2.2) than

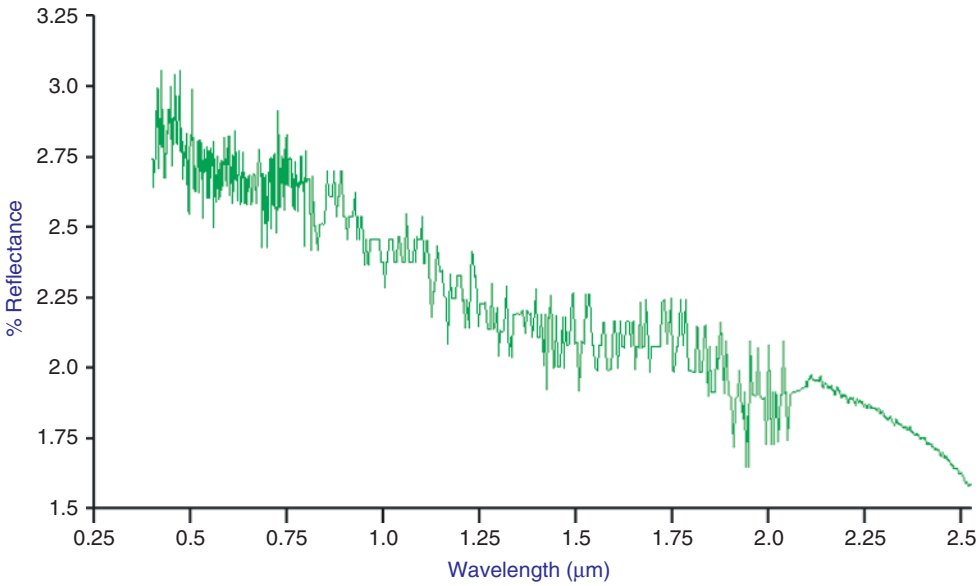

Figure 1.26 *Reflectance spectrum of tap water from 0.4 to 2.55 µm. Data from the ASTER spectral library through the courtesy the Jet Propulsion Laboratory, California Institute of Technology,Pasadena, California,* © *California Institute of Technology. All rights reserved.*

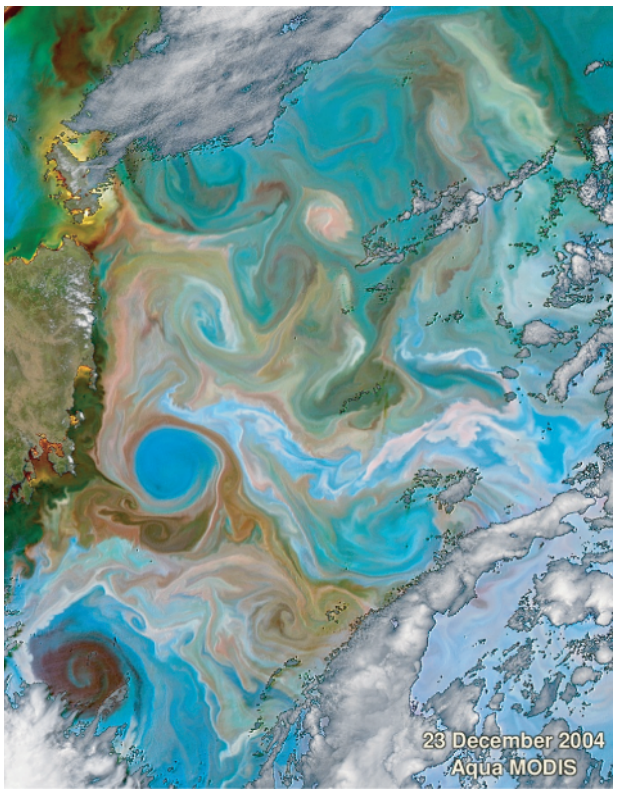

Figure 1.27 *This image of the ocean east of Tasmania in December, 2004 depicts subtle differences in water colour that result from varying distributions of such scattering and absorbing agents in the water column as phytoplankton, dissolved organic matter, suspended sediment, bubbles, and so on. The ocean colours shown above result from independently scaling the satellite-derived normalised water-leaving radiances (nLw) at 551, 488 and 412 nm and using the results as the red, green and blue components of the image, respectively. Differences in the colours may also partially reflect differences in atmospheric components or levels of sun and sky glint or differences in the path that light takes through the MODIS instrument. The MODIS instrument is described in Section 2.3. Source: http://oceancolor.gsfc.nasa.gov/cgi/image_archive.cgi?c =CHLOROPHYLL. Image courtesy of NASA/USGS.*

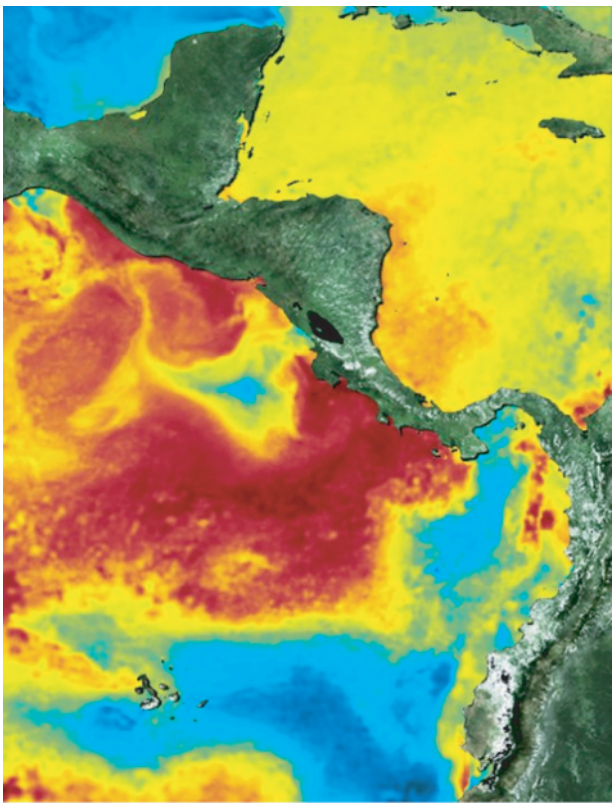

Figure 1.28 *Surface temperature image of the seas around the Galapagos and Cocos Islands. This heat map, produced through ESA's Medspiration project, shows the sea surface temperatures around Galapagos Islands and Cocos Island in the Pacific Ocean for 18 March 2007 using data from the AATSR sensor carried by the ENVISAT satellite (Section 2.2.1). Reproduced with permission from http://dup.esrin.esa.it/news/inews/inews_130.asp.*

would be required to detect suspended sediment. Furthermore, the level of backscatter from chlorophyll is lower than that produced by suspended sediment; consequently, greater radiometric sensitivity is also required. Ocean observing satellites (Section 2.2.4) carry instruments that are 'tuned' to specific wavebands that match reflectance peaks or absorption bands in the spectra of specific materials such as chlorophyll.

Although the spectral reflectance properties of suspended matter and chlorophyll have been described separately, it is not uncommon to find both are present at one particular geographical locality. The complications in separating-out the contribution of each to the total observed reflectance are considerable. Furthermore, the suspended matter or chlorophyll may be unevenly distributed in the horizontal plane (the patchiness phenomenon noted above) and in the vertical plane. This may cause problems if the analytical technique used to determine concentration levels from recorded radiances is based on the assumption that the material is uniformly mixed at least to the depth of penetration of the radiation. In some cases, a surface layer of suspended matter may ride on top of a lower, colder, layer with a low suspended matter concentration, giving rise to considerable difficulty if standard analytical techniques are used. Reflection from the bed of the water body can have unwanted effects if the primary aim of the experiment is to determine suspended sediment or chlorophyll concentration levels, for it adds a component of reflection to that resulting from backscatter from the suspended or dissolved substances. In other instances, collection of the EMR reflected from the sea bed might

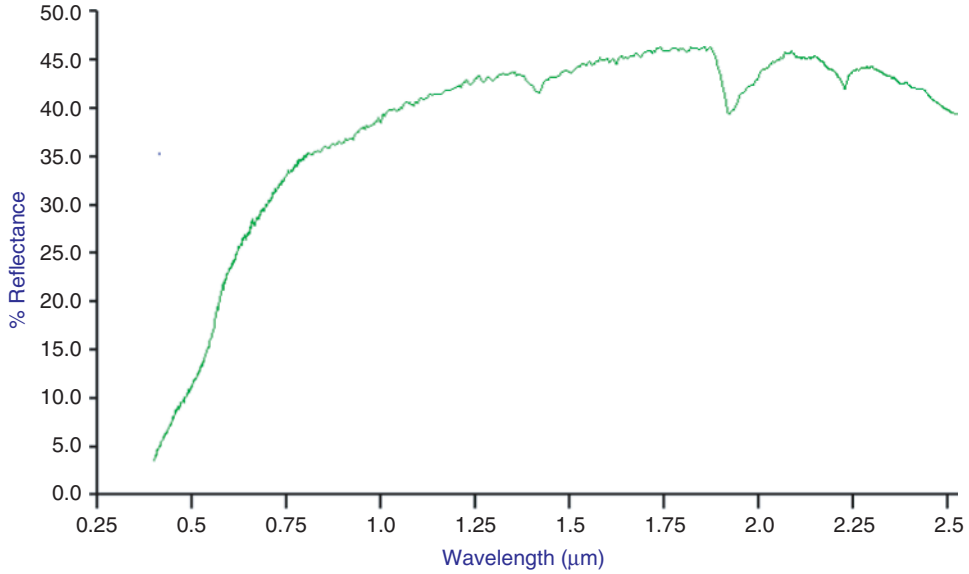

Figure 1.29 *Reflectance spectrum of a brown fine sandy loam soil from 0.4 to 2.5 μm. Note that the y-axis is graduated in percentage reflection. Soil spectra vary with the mineralogical properties of the soil and also its moisture status. The latter varies temporally and spatially. Data from the ASTER spectral library through the courtesy the Jet Propulsion Laboratory, California Institute of Technology,Pasadena, California,*

be the primary focus of the exercise, in which case the presence of organic or inorganic material in the water would be a nuisance.

The reflectance spectrum of clear water can be inferred from Figure 1.24a. The magnitude of reflected radiation is low, with absorption increasing with wavelength so that in the NIR region of the spectrum absorption is almost total, and water appears black in the image. Indeed, one of the methods of estimating the atmospheric contribution to the signal received at the sensor is to look at the recorded radiance for a deep clear lake in the NIR. The departure from zero is an estimate of the atmospheric path length (Figure 1.24b). The spectral reflectance curve for tap water is shown in Figure 1.26.

One of the main interests of satellite oceanography is in the derivation of images showing patterns in the oceans and seas of the world. Ocean colour is a term used to describe the variability in colour in images. Figure 1.27 is an example. Ocean colour is related to oxygen consumption and can help in, for example guiding fishing fleets to their prey. A second, important, area of satellite oceanography is the study of SST distribution. Figure 1.28 is an example of a SST image.

1.3.2.4 Soils

The spectral reflectance curves of soils (Figure 1.29) are generally characterized by a rise in reflectivity as wavelength increases – the opposite, in fact, of the shape of the spectral reflectance curve for water. Reflectivity in the visible wavebands is affected by the presence of organic matter in the soil, and by the soil moisture content, while at 0.85–0.93 μm there is a ferric iron absorption band. As ferric iron also absorbs ultraviolet radiation in a broad band, the presence of iron oxide in soils is expressed visually by a reddening of the soil, the redness being due to the absorption of the wavelengths shorter (and longer) than the red. Between 1.3–1.5 and 1.75–1.95 μm water absorption bands occur, as mentioned in Section 1.2.5. Soil reflectance in the optical part of the electromagnetic spectrum is usually greatest in the region between these two water absorption bands, and declines at wavelengths longer than 2 μm with clay minerals, if present, being identifiable by their typical narrow-band absorption features in the 2.0–2.5 μm region. Irons, Weismiller and Petersen (1989) provide a comprehensive survey of factors affecting soil reflectance. Huete (1989) gives a summary of the influence of the soil background on measurements of vegetation spectra, while Huete (2004) is a good review of the remote sensing of soils and soil processes.

1.4 Summary

In the opening paragraph of Section 1.3.2.1, a basic principle of applied remote sensing is set out. This states that individual Earth-surface cover types are distinguishable in terms of their spectral reflection and emission characteristics. Changes in the spectral

response of objects can also be used as an indication of changes in the properties of the object, for example the health or growth stage of a plant or the turbidity of a water body. In this chapter, the basic principles of EMR are reviewed briefly, and the relevant terminology is defined. An understanding of these basic principles is essential if the methods described in the remainder of this book are to be applied sensibly. Chapter 2 provides details of the characteristics of sensors that are used to measure the magnitude of EMR that is reflected from or emitted by the Earth surface. It is from these measurements that the spectral reflectance curves of Earth surface elements can be derived. Further details of the derivation of absolute spectral reflectance values from remotely-sensed measurements are provided in Chapter 4, while the use of data from imaging spectrometers, which can record data in tens or hundreds of bands, is described in Chapter 9. However advanced the processing techniques are, their results cannot be properly understood if the user does not have a good working knowledge of the material covered in Chapter 1. Readers are encouraged to consult the main references given in the text, and to familiarize themselves with the reflection spectra of natural targets, for example by using the MIPS software that can be downloaded from the publisher's web site at URL www.wiley.com/go/mather4. MIPS contains a small spectral library which is accessed from the *Plot|Plot Library Spectrum* menu. It includes a selection of spectra from the ASTER spectral library (with the permission of the Jet Propulsion Laboratory, California Institute of Technology, Pasadena, CA, USA).